Enhancement of Handover Management Through Reconfigurable Intelligent Surfaces in a 3D Ground-Aerial-Space Network Scenario

Anna Maria Vegni, *Senior Member, IEEE*, Yalçın Ata, *Senior Member, IEEE*, and Mohamed Slim Alouini, *Life Fellow, IEEE*

***Abstract*— This paper investigates the role of reconfigurable intelligent surface (RIS) for enhanced handover management in 6G networks with overlapping wireless network layers *i.e.*, ground, aerial, and space. A high altitude platform system (HAPS) is equipped with RIS and the comparison of direct and RIS-assisted link performance is presented. To do this, the average bit error rate, the outage probability (OP), and the channel capacity of direct and HAPS-assisted links are obtained in closed form expressions. By estimating the link error probability, a novel handover mechanism exploits the use of RIS, resulting in enhanced connectivity management. Hard and soft handover modes are defined depending on the radio frequency (RF) connectivity by means of link error threshold. The decision for the handover execution is based on selecting the optimal link among multiple available ones from ground, aerial, and space layers. The performance of RIS-assisted handover mechanism has been compared to traditional hard and soft handover procedure, as well as link performance achieved with relay node. Numerical and simulation results reveal that the connectivity of a user equipment can be maintained through RIS-aided links in case of any performance degradation in the direct RF links. Particular scenarios highlight that the use of RIS for handover is preferred to traditional handover procedures, as well as relay nodes.**

***Index Terms*— Reconfigurable intelligent surfaces, handover management, 3D connectivity, 6G.**

I. Introduction

In 6G network scenarios, the use of reconfigurable intelligent surfaces (RISs) is expected to dominate as an effective communication tool that enhances link performance. RIS main feature is their ability to control signal propagation by exploiting scattered, reflected, and refracted signals toward a specific destination [1], [2]. Traditionally, RISs find large utilization for blockage avoidance, in order to support link disconnections caused by obstructions (*e.g.*, buildings or any other obstacle) by easily using reflected signals on the intelligent surface. Indeed, RISs are nearly passive devices [3] that are designed to control the impinging signal by adjusting the phase, and redirect the beam toward a desired destination. More in details, an RIS is a smart thin material sheet (broadly speaking, a wallpaper), which covers parts of walls, buildings, ceilings, etc., and acts as a relay node that redirects a controlled and modified signal.

There exist many other applications of RISs, not limited to blockage avoidance, ranging from coverage enhancement to interference suppression, as well as from radio localization to power transfer and security aspects [4]. All these applications refer to both indoor and outdoor scenarios, thus creating smart radio environments. Focusing to outdoor applications, RISs are employed for controlling connectivity links and manage handover mechanisms for mobile users, such as vehicles [5], [6]. In a heterogeneous network environment, with multiple available wireless links, it is possible to enhance link performance in case of degradation or disconnections. Traditional handover procedure, originally conceptualized for cellular networks, is a critical process in mobile networks, by providing the ability to maintain the service active while a user equipment (UE) is moving, or the serving link is in outage. Handover is expected to benefit from RISs. Indeed, connectivity links exploiting RIS elements usually present better performance than direct links; it is then possible to switch from a direct link to a no direct RIS-enhanced one in order to enhance the performance. In this case, the handover procedure will only change the path from the transmitter to the receiver and not the transmitter node, as traditionally occurs in cellular network handovers where the connectivity link switches from a *serving cell* to a *new candidate one* [7]. This configuration allows to reduce the traffic overhead of handover management, as well as maintain the same transmitter node, thus providing security enhancement.

Starting from traditional handover procedure, both for hard and soft mode, we aim to integrate RIS-embedded devices to reinforce handover procedure. Focusing on a 3D network

Received 6 February 2024; revised 17 June 2024 and 30 August 2024; accepted 27 September 2024. Date of publication 8 October 2024; date of current version 12 December 2024. This work was supported in part by European Cooperation in Science and Technology (COST) Action NEWFOCUS under Grant CA19111. The associate editor coordinating the review of this article and approving it for publication was W. Hamouda. *(Corresponding author: Anna Maria Vegni.)*

Anna Maria Vegni is with the Department of Industrial, Electronics and Mechanical Engineering, Roma Tre University, 00154 Rome, Italy (e-mail: annamaria.vegni@uniroma3.it).

Yalçın Ata is with the Department of Electrical and Electronics Engineering, OSTIM Technical University, Yenimahalle, 06374 Ankara, Türkiye (e-mail: ylcnata@gmail.com).

Mohamed Slim Alouini is with the Computer, Electrical and Mathematical Science and Engineering Division, King Abdullah University of Science and Technology (KAUST), Thuwal 23955, Saudi Arabia (e-mail: slim.alouini@kaust.edu.sa).

Color versions of one or more figures in this article are available at https://doi.org/10.1109/TWC.2024.3471393.

Digital Object Identifier 10.1109/TWC.2024.3471393

scenario, that is a wireless network environment comprised of ground, aerial, and space layers, in this paper we assume an RIS-embedded device on the aerial layer [8], providing downlink connectivity respectively from space-to-ground and from ground-to-ground paths. Specifically, we assume high altitude platform systems (HAPS) are coated with an RIS with variable number of reconfigurable elements. HAPS are then deployed to redirect wireless signals impinged on the RIS, which have been transmitted from a ground station or a satellite.

We present an handover mechanism comparing the link performance for both line of sight (LoS) and no line of sight (NLoS) links. For different connectivity links we derive the associated performance, expressed as average bit error rate (BER) variation, outage probability (OP), as well as channel capacity. Based on performance comparison, our handover mechanism will compute the probability of executing an handover for different connectivity links. Numerical results will show higher handover probabilities for connectivity switching towards RIS-assisted NLoS paths, than simple relay nodes. Also, a performance improvement is observed for an increasing number of RIS elements, but for very high values no significant impact is observed.

In this paper, we address how to strength traditional handover management with the use of RISs. We distinguish different cases where RISs can effectively enhance the link performance. More in details, considering an overlapping ground-aerial-space environment where a HAPS is embedded with a RIS device, we derive the RIS-aided handover probabilities, which are compared to both the traditional handover that does not consider the use of RISs, as well as active relay-based links. An algorithm for RIS-based handover is then presented, where link performance (*i.e.*, the average BER) is the metric for handover triggering. Specifically, the following goals will be addressed in this paper:

- We investigate the role of RIS for enhanced handover management in 6G wireless networks, by comparing the performance associated to different LoS and RIS-aided NLoS connectivity links that may exist in a ground-aerial-space network scenario;
- We develop a new handover decision algorithm covering the RIS effect and benefiting the improving effect of RIS in handover management. Handovers occur both in hard and soft mode, and are triggered based on link performance such as the BER;
- We define the handover probabilities with and without the use of RISs, taking into account different direct and no direct links, and comparing to the case of a simple relay node with Amplify-and-Forward (AF) mode, so that the signal is amplified and then re-transmitted;
- We extend the achieved derivations of BER, OP, and channel capacity to high signal-to-noise ratio (SNR) regime, thus showing the asymptotic analysis, together with the diversity order;
- We distinguish different scenarios where the use of RISs can effectively provide a benefit for handover management, such as in case of the negative ping-pong effect or to reduce the traffic load of a wireless network;
- We present the results of the handover probability able to maintain the connectivity of the UE at lowest level of error probabilities with the help of RIS application. Monte Carlo (MC) simulations are carried out in order to assess the achieved numerical results.

This paper is organized as follows. Section II deals with some recent works on the use of RISs for handover management. In Section III we introduce the proposed 3D scenario comprised of ground, aerial, and space network layers, where an RIS-embedded HAPS device is used as relay node toward the end user laying on the ground. Section IV and Section V analyse respectively the radio frequency (RF) and RIS-assisted RF (RRF)-assisted links and derive the associated average BER, the OP, as well as the channel capacity. In Section VI, the asymptotic analysis for the average BER and OP in high SNR regime has been carried out. Our proposed RIS-based handover approach is described in Section VII, where we derive the handover probabilities in case of no-RIS direct links and with the support of RIS-embedded devices. Numerical results are carried out in Section VIII. It will be easy to notice the benefits of RIS-based connectivity links expressed as an increase of achieved capacity, as well as the increasing number of RIS elements can reduce the OP. The handover probability occurring in hard and soft mode will be compared through numerical and simulation results. Our findings reveal that the probability of hard RIS-based handover is higher when the number of RIS elements increases, while for soft RIS-based handover the associated probability is smaller, meaning that the benefit is limited as compared to hard RIS-based handover. Particular scenarios, highlighting the importance of the role of RIS for handover, are also investigated. Finally, conclusions are drawn in Section IX.

II. Related Works

The use of RISs in wireless networks has been largely adopted thanks to their ability to reconfigure the signal features accordingly, for instance, in order to extend the radio coverage in case of blockages that do not allow data reliability. Leveraging on the intrinsic nature of RISs, they are expected to revolutionize the handover management in next generation wireless networks, so that alternative reflecting connectivity links can be built on the need. Traditional handovers allow the connectivity switching from a serving access point (AP) to a candidate one, chosen according to different metrics, such power, quality of service, interference, etc. When a handover is executed, traffic overhead occurs due to authentication, authorization and access phase needed to register the UE to the new serving AP. So, avoiding unnecessary and unwanted handovers is a challenge that needs to be achieved to reduce energy consumption at the UE, as well as network overhead. For instance, when a UE is at the borderline of a cellular network, small fluctuations of received power level forces the UE to switch from a serving cell to a neighboring one, causing the unwanted ping-pong effect.

Thanks to the feature of accordingly reflecting beamforming coming from a serving base station (BS) via adjustable phase shift, RISs are expected to support handover management.

RIS-aided connectivity links result as alternative connectivity links, since allow to reach the UE even when the direct link from a BS is not available, as well as shows low performance. It is then interesting to investigate when to use RIS-aided connectivity links as alternative to traditional handover occurrences, as well as in conjunction to direct links resulting as a soft handover procedure.

The topic of RISs for handover management is quite recent and at today a few works are investigating on this direction. In [9], the authors present several handover (HO) optimization technique solutions for beyond 5G (B5G). Among the potential technologies that can help in enhancing the HO optimization in B5G, RISs have a relevant role. For this aim, RISs are exploited to either recover the channel blockage or facilitate UE handover. This aspect has been recently investigated in [10], by proposing a handover procedure for blockage avoidance in case of Visible Light Communication (VLC) indoor scenarios. Also, the use of RIS for handover management allows to reduce the cumulative handover overhead by jointly adjusting beamformers and RIS phase shifts, and achieves higher spectrum efficiency. In [11], it is proved that RISs can serve as an alternative approach to combat the blockage effect and largely reduce the number of handovers triggered by frequent channel blockages.

Deb et al. [12] investigate how to choose an appropriate BS or a BS-RIS link to maximise user throughput under reliability and latency constraints, based on the formulation of a multi-armed bandit problem. Wei and Zhang [13] investigate the handover probability in case of RIS-aided networks, and evaluated the optimal distributed RIS deployment that minimizes the handover probability. Finally, in [14], Hedhly et al. present an inner tube network architecture for seamless and reliable connection, where a RIS is strategically positioned along the tube to improve the wireless cell coverage. The authors also exploit the design of a soft handover scheme for the inner-tube wireless network.

Differently from previous works, which focus on novel handover techniques aided by RIS, in this paper we investigate the role of RISs for handover management in 6G scenario, by comparing traditional (*i.e.*, no RIS) and RIS-assisted handover. We are interested in investigating if and when RISs are more convenient to exploit than using a simple relay node. In next sections, we will investigate the channel models in case of direct RF links and no-direct RIS-based ones. Our proposed handover algorithm will exploit the link metrics that trigger a handover. We will observe the effectiveness of RIS-based handover to enhance connectivity management, especially for high number of RIS elements, as compared to traditional (*i.e.*, no RIS) handover procedure. As a result, the handover procedure that basically consists in switching from a serving BS to a candidate one via direct links, can be revised by exploiting RIS-aided NLoS links, while maintaining the same transmitting node.

III. System Model

Let us consider the reference scenario depicted in Fig. 1. Overlapping wireless networks are coexisting, so that an UE can receive multiple links from different sources. Specifically,

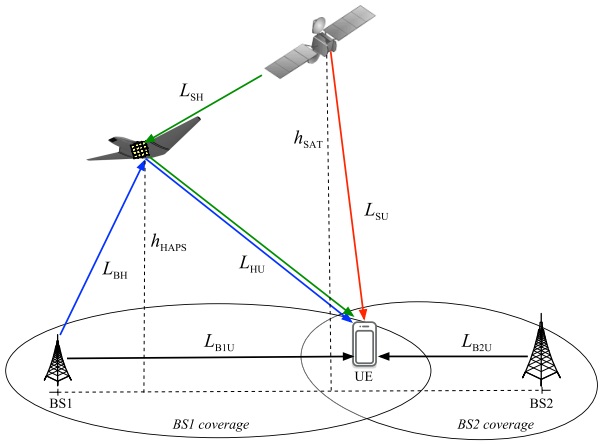

Fig. 1. Schematic of overlapping ground, aerial, and space network layers for handover management. HAPS are RIS-equipped and act as relay node from ground and space layers. Ground-to-ground links (*black lines*) and space–to-ground (*red line*) are direct links, while ground-to-aerial-to-ground (*blue lines*) and satellite-to-aerial-to-ground (*green lines*) are no direct RIS-based paths.

we assume multiple RF BS in the ground network, each with a given radio coverage and transmitting a given power level. The UE is in a given position, so that L_{B1U} [m] and L_{B2U} [m] are its distance to BS1 and BS2, respectively. The connectivity links from the ground stations to the UE are in LoS.

On the aerial layer, a RIS-embedded HAPS is laying at a fixed altitude from the ground *i.e.*, h_{HAPS} [m]. The role of HAPS is fundamental in our reference scheme as it interconnects the ground network in case of disconnections or for handover management, as well as provides connectivity from the satellite to the UE. Specifically, we assume the RIS module has a number of $\mathcal{N}$-elements reflecting surfaces and it is used as a relay providing two additional NLoS links between BS-UE and satellite (SAT)-UE, depending on the impinging wireless signal. Indeed, the wireless signal transmitted by BS1 to HAPS propagates along L_{BH} [m] and L_{HU} [m] links till reaching the UE. On the other side, in the space layer a satellite is at altitude h_{SAT} [m] and provides RF direct link to the UE assuming a distance of L_{SU} [m], as well as redirects the signal through the RIS-embedded HAPS along L_{SH} [m] and L_{HU} [m] links.

The UE is primarily connected to the BSs. The handover management is performed based on the assessment of the error probabilities of the five links given in Fig. 1. All the RF fading channels are assumed to follow Nakagami-m distribution, with different parameters as detailed in the following. While the error probability of direct BS-UE link falls below the defined error threshold, hard and soft handovers are done by selecting the optimal link according to developed algorithms among the configurations given in Fig. 1. Specifically, we distinguish among (*i*) traditional (hard/soft) handover procedure, (*ii*) handover through relay-based no-direct paths, and (*iii*) handover through RIS-based no-direct paths. As depicted in Fig. 2, let us assume BS1 is a serving AP, experiencing link degradation that triggers a handover procedure in order to maintain the service active. A traditional handover mechanism consists in direct links from a transmitter to the UE, breaking the serving

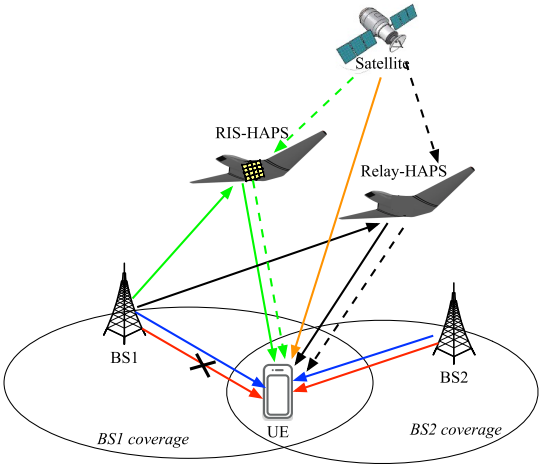

Fig. 2. Comparison of different handover mechanisms. For ground connectivity, we consider (*i*) traditional hard (*red links*) and soft (*blue links*) handover, (*ii*) path through no-direct RIS-embedded HAPS (*solid green links*), and (*iii*) path through no-direct relay-HAPS (*solid black links*). For satellite connectivity (*orange link*), we consider (*i*) path through no-direct RIS-embedded HAPS (*dashed green links*), and (*ii*) path through no-direct relay-HAPS (*dashed black links*).

connection and switching to a candidate one in case of hard handover (red links), or combining multiple direct links in case of soft handover (blue links). In contrast, BS1 can reach the UE through a no-direct path by relying on HAPS, which can be embedded with RIS (green path) or not. In the latter case, the HAPS simply acts as a relay node (black path). In this paper, we are interested in assessing the handover probability in case of traditional procedures (*i.e.*, hard/soft classic handover, as well as no-direct relay-based path) and novel RIS-based approach. Notice that for satellite link (orange link), the handover procedure will rely on no-direct paths with HAPS, acting as relay (dashed black path) or RIS-embedded node (dashed green path).

IV. RF LoS Link Analysis

This section focuses on the analytical modeling of RF direct LoS links. According to Fig. 1, we consider a RF point-to-point transmission, such as the ground-to-ground link or the SAT-to-UE link. Assuming the Nakagami-m distribution [15] for each RF link, it is easy to derive the expression of SNR and from there the average BER, the OP, as well as the channel capacity.

For a given RF LoS link, the received signal can be written by [16]

$$y_{RF} = \sqrt{P_t}\sqrt{g}h_{RF}\sqrt{E_s}x + n_0, \tag{1}$$

where P_t [W] is the transmitted power, g [W] is the average power gain, E_s is the energy per symbol, and n_0 is the zero-mean Gaussian noise. The associated instantaneous SNR can be expressed as

$$\gamma_{RF} = \overline{\gamma}_{RF} h_{RF}^2, \tag{2}$$

where $\overline{\gamma}_{RF}$ [dB] is the average SNR of RF link, defined as $\overline{\gamma}_{RF} = P_t g E_s/\sigma_n^2$, with σ_n^2 as the noise variance.

A. Average BER

According to the Nakagami-m distribution adopted to model the RF channel, the probability density function (PDF) of the instantaneous SNR can be written as

$$f_{\gamma_{RF}}(\gamma_{RF}) = \left(\frac{m}{\overline{\gamma}_{RF}\Omega}\right)^m \frac{\gamma_{RF}^{m-1}}{\Gamma(m)} \exp\left(-\frac{m}{\overline{\gamma}_{RF}\Omega}\gamma_{RF}\right), \tag{3}$$

where $\gamma_{RF} \geqslant 0$, $m = \frac{(E[h_{RF}^2])^2}{Var(h_{RF}^2)}$ is the shape parameter that denotes the fading severity, with $E[\cdot]$ as the expected value and $Var(\cdot)$ as the variance, and $\Omega = E[h_{RF}^2]$ is the spread parameter that implies the mean power.

The probability error (BER) of an intensity modulation/direct detection (IM/DD) on-off keying (OOK) system can be found as $P_b(e) = p(1)p(e|1) + p(0)p(e|0)$, where $p(0)$ and $p(1)$ are the probability of sending bits 0 and 1, and $p(e|0)$ and $p(e|1)$ are the probability of error after sending bits 0 and 1, respectively. Assuming that bits 0 and 1 are equiprobable and then, $p(e|0) = p(e|1)$, the conditioned probability will result as [17]

$$P_b(e|\gamma) = Q\left(\sqrt{\gamma/2}\right) = \text{erfc}\left(\sqrt{\gamma}/2\right)/2, \tag{4}$$

where $Q(\cdot)$ is the Q-function, $\text{erfc}(x)$ is the complementary error function, and $Q(\sqrt{2}x) = \text{erfc}(x)/2$. It follows that the average BER of the RF link can be obtained as

$$BER_{RF} = \int_0^\infty P_b(e|\gamma_{RF}) f_{\gamma_{RF}}(\gamma_{RF}) d\gamma_{RF}, \tag{5}$$

which after some rearrangements becomes

$$BER_{RF} = \frac{1}{2\Gamma(m)}\left[\Gamma(m) - \frac{\Gamma(m+1/2)\sqrt{\Omega\overline{\gamma}_{RF}}}{\sqrt{\pi m}} \times {}_2F_1\left(\frac{1}{2}, m+\frac{1}{2}; \frac{3}{2}; -\frac{\Omega\overline{\gamma}_{RF}}{4m}\right)\right], \tag{6}$$

where ${}_2F_1(.)$ is the hypergeometric function.

B. Outage Probability

From the expression of the instantaneous SNR γ_{RF}, the associated cumulative distribution function (CDF) for the RF link is found by

$$F_{\gamma_{RF}}(\gamma_{RF}) = 1 - \int_{\gamma_{RF}}^\infty f_{\gamma_{RF}}(x)dx, \tag{7}$$

and inserting Eq. (3) into Eq. (7), we have

$$F_{\gamma_{RF}}(\gamma_{RF}) = 1 - \frac{(m/\Omega)^m}{\Gamma(m)\overline{\gamma}_{RF}^m} \int_{\gamma_{RF}}^\infty x^{m-1} e^{\left(-\frac{mx}{\Omega\overline{\gamma}_{RF}}\right)} dx. \tag{8}$$

Using [18, Eq. (3.351-2)], it is possible to derive the CDF and then the OP, defined as the probability of the instantaneous SNR γ_{RF} falls below the defined SNR threshold $\gamma_{RF_{th}}$, *i.e.*,

$$P_{out,RF} = P_r(\gamma_{RF} \leqslant \gamma_{RF_{th}}) = F_{\gamma_{RF}}(\gamma_{RF_{th}}), \tag{9}$$

that can be expressed as

$$P_{out,RF} = 1 - \frac{1}{\Gamma(m)}\Gamma\left(m, \frac{m}{\Omega\overline{\gamma}_{RF}}\gamma_{RF_{th}}\right), \tag{10}$$

where $\Gamma(a,b)$ is the upper incomplete gamma function.

C. Channel Capacity

The channel capacity for RF link can be found by [19]

$$C_{RF} = \frac{1}{\ln(2)} \int_0^\infty \ln\left(1+\gamma_{RF}\right) f_{\gamma_{RF}}(\gamma_{RF}) d\gamma_{RF}. \quad (11)$$

First using [20, Eq.(11)] then, applying [21, Eq. (07.34.21.0011.01)] the channel capacity of RF link becomes

$$C_{RF} = \frac{1}{\ln(2)\Gamma(m)} G_{3,2}^{1,3}\left(\frac{\Omega\overline{\gamma}_{RF}}{m}\middle|\begin{matrix}1,1,1-m\\1,0\end{matrix}\right), \quad (12)$$

where $G_{a,b}^{c,d}$ is the Meijer-G function.

V. RIS-Assisted RF Link Analysis

From Fig. 1, we are now focusing on NLoS paths that involve the use of RIS-embedded HAPS. Specifically, we will derive the average BER, the OP, and the channel capacity associated to such paths, defined as RRF links. In this paper, we work in the far-field propagation scenario with plane wave-front assumption, as the distance between the RIS-embedded device and the transmitter/receiver is far beyond the Rayleigh distance, expressed as $2\mathcal{M}^2/\lambda$, with $\mathcal{M}$ [m] as the dimension of the RIS elements, and λ [m] as the carrier wavelength. The assumption of working in a far-field scenario in also supported by a limited number of RIS elements (*i.e.*, $\mathcal{N}$), as assumed in this paper. However, in case of larger number of RIS elements, the Reileigh distance will be larger than the distance from the transmitter to the receiver, and then the near-field scenario should be considered. The investigation on the correct working scenario (*i.e.*, near- or far-field) is addressed in [22], where the RIS is dynamically partitioned into sub-arrays, each consisting of several RIS units, so that for each sub-array the far-field condition holds. A RIS-assisted RF link through $\mathcal{N}$-elements reflecting surfaces will yield a signal at the receiver plane expressed as

$$y = \sum_{r=1}^{\mathcal{N}} h_r \mathcal{B}_r \exp(\imath\theta_r) g_r x + n_0, \quad (13)$$

where $\imath = \sqrt{-1}$, $h_r = v_r \exp(-\imath\varphi_r)$ and $g_r = u_r \exp(-\imath\phi_r)$ are the gain of first (*i.e.*, link from source to HAPS) and second (*i.e.*, link from HAPS to UE) channels, and φ_r and ϕ_r are the phase shifts of the transmitted signal x along the first and second path, respectively. Furthermore, $\mathcal{B} \in [0,1]$ is the reflection amplitude, $\theta_r \in [0, 2\pi]$ is the phase shift induced by the reflecting meta-surface, and $\mathcal{N}$ is the number of reflecting elements on the HAPS. Notice that in the most general case of imperfect channel state information (CSI), the phase shift should be considered and the instantaneous SNR becomes

$$\gamma_{RRF} = \frac{\left(\sum_{r=1}^{\mathcal{N}} v_r u_r \exp[\imath(\theta_r - \varphi_r - \phi_r)]\right)^2 \mathcal{B}^2 P_t^2}{\sigma_r^2}, \quad (14)$$

where all the reflecting surfaces are assumed identical with the same reflection coefficient as $\mathcal{B}_r = \mathcal{B}$. In the following, we assume that SNR is maximum by setting $\theta_r - \varphi_r - \phi_r = 0$ in Eq. (14), then the instantaneous SNR can be arranged as

$$\gamma_{RRF} = \left(\sum_{r=1}^{\mathcal{N}} v_r u_r\right)^2 \mathcal{B}^2 P_t^2/\sigma_r^2, \quad (15)$$

and expressing the average SNR as $\overline{\gamma}_{RRF} = P_t^2/\sigma_r^2$, Eq. (15) becomes

$$\gamma_{RRF} = \left(\sum_{r=1}^{\mathcal{N}} v_r u_r\right)^2 \mathcal{B}^2 \overline{\gamma}_{RRF} = \left(\sum_{r=1}^{\mathcal{N}} \mathcal{H}_r\right)^2 \mathcal{B}^2 \overline{\gamma}_{RRF}. \quad (16)$$

According to [23], the term $\mathcal{H}_r = v_r u_r$ is the product of two Nakagami-m random variables (RVs) (*i.e.*, v_r and u_r), each with a PDF given as

$$f_{\mathcal{V}_r,\mathcal{U}_r}(v_r,u_r) = \frac{2\left(\frac{m_{1,2}^{m_{1,2}}}{\Omega_{1,2}^{m_{1,2}}}\right)}{\Gamma(m_{1,2})} (v_r,u_r)^{2m_{1,2}-1} \times \exp\left(-\frac{m_{1,2}}{\Omega_{1,2}}(v_r,u_r)^2\right), \quad (17)$$

where subscripts 1 and 2 refer to the two RVs, with m and Ω denoting the shape and spread parameters defined in [15]. The product of two Nakagami-m distributions can be expressed by the double Nakagami-m distribution as [24]

$$f_{\mathcal{H}_r}(h_{RRF}) = \frac{4h_{RRF}^{m_1+m_2-1} K_{m_1-m_2}\left(2h_{RRF}\prod_{i=1}^{2}\sqrt{\frac{m_i}{\Omega_i}}\right)}{\prod_{i=1}^{2}\Gamma(m_i)\left(\frac{\Omega_i}{m_i}\right)^{\frac{m_1+m_2}{2}}}, \quad (18)$$

where $K_a(\cdot)$ is the second kind modified Bessel function with order a. Also, assuming that double Nakagami-m RVs $\mathcal{H}_1, \mathcal{H}_2, \ldots, \mathcal{H}_{\mathcal{N}}$ are independent and not necessarily identically distributed (i.ni.d.), so that $\mathcal{H}_1 = \mathcal{H}_2 = \ldots = \mathcal{H}_{\mathcal{N}} = \mathcal{H}$, and according to [25] the sum of these random variables $\sum_{r=1}^{\mathcal{N}} \mathcal{H}_r$, with $r = 1, \ldots, \mathcal{N}$, can be approximated to the Gamma distribution (when $\mathcal{N} \geqslant 2$) *i.e.*,

$$f_{\mathcal{H}}(h_{RRF}) = \frac{h_{RRF}^{\zeta_1}}{\Gamma(\zeta_1+1)\zeta_2^{\zeta_1+1}} \exp\left(-\frac{h_{RRF}}{\zeta_2}\right), \quad (19)$$

where $\zeta_1 = \frac{(E[\mathcal{H}])^2}{Var[\mathcal{H}]} - 1$ and $\zeta_2 = \frac{Var[\mathcal{H}]}{E[\mathcal{H}]}$, with $E[\cdot]$ as the mean value and $Var[\cdot]$ as the variance, which can be written respectively as

$$E[\mathcal{H}] = \mathcal{N}\left(\frac{\Omega_1\Omega_2}{m_1 m_2}\right)^{1/2} \frac{\Gamma(m_1+1/2)\Gamma(m_2+1/2)}{\Gamma(m_1)\Gamma(m_2)}, \quad (20)$$

$$Var[\mathcal{H}] = \left[1 - \frac{1}{m_1 m_2}\left(\frac{\Gamma(m_1+1/2)\Gamma(m_2+1/2)}{\Gamma(m_1)\Gamma(m_2)}\right)^2\right] \times \mathcal{N}\Omega_1\Omega_2. \quad (21)$$

It follows that the SNR expression becomes

$$\gamma_{RRF} = \overline{\gamma}_{RRF}\mathcal{N}^2\mathcal{B}^2\mathcal{H}^2. \quad (22)$$

The PDF of the instantaneous SNR will be obtained by using

$$f_{\gamma_{RRF}}(\gamma_{RRF}) = f_{\mathcal{H}}\left(\frac{\sqrt{\gamma_{RRF}}}{\sqrt{\overline{\gamma}_{RRF}}\mathcal{N}\mathcal{B}}\right)\left|\frac{d\mathcal{H}}{d\gamma_{RRF}}\right|, \quad (23)$$

where $\mathcal{H}$ is given from Eq. (22) as $\mathcal{H} = \frac{\sqrt{\gamma_{RRF}}}{\sqrt{\overline{\gamma}_{RRF}}\mathcal{NB}}$, and then

$$\frac{d\mathcal{H}}{d\gamma_{RRF}} = \frac{1}{2\sqrt{\overline{\gamma}_{RRF}\gamma_{RRF}}\mathcal{NB}}. \tag{24}$$

Finally, using Eqs. (17) and (22) in Eq. (23), it leads to

$$f_{\gamma_{RRF}}(\gamma_{RRF}) = \frac{\gamma_{RRF}^{\frac{\zeta_1-1}{2}}}{2\left(\zeta_2\sqrt{\overline{\gamma}_{RRF}}\mathcal{NB}\right)^{\zeta_1+1}\Gamma(\zeta_1+1)} \times \exp\left(-\frac{\sqrt{\gamma_{RRF}}}{\zeta_2\sqrt{\overline{\gamma}_{RRF}}\mathcal{NB}}\right). \tag{25}$$

A. Average BER

Inserting Eqs. (4) and (25) into Eq. (5), the average BER will be

$$BER_{RRF} = \frac{1}{4\left(\zeta_2\sqrt{\overline{\gamma}_{RRF}}\mathcal{NB}\right)^{\zeta_1+1}\Gamma(\zeta_1+1)} \times \int_0^\infty \gamma_{RRF}^{\frac{\zeta_1-1}{2}} \operatorname{erfc}\left(\frac{\sqrt{\gamma_{RRF}}}{2}\right) e^{\left(-\frac{\sqrt{\gamma_{RRF}}}{\zeta_2\sqrt{\overline{\gamma}_{RRF}}\mathcal{NB}}\right)} d\gamma_{RRF}. \tag{26}$$

By exploiting the following variable transformation *i.e.* $\sqrt{\gamma_{RRF}} = x$, we have $d\gamma_{RRF} = 2xdx$, and Eq. (26) becomes

$$BER_{RRF} = \frac{1}{2\left(\zeta_2\sqrt{\overline{\gamma}_{RRF}}\mathcal{NB}\right)^{\zeta_1+1}\Gamma(\zeta_1+1)} \int_0^\infty x^{\zeta_1} \operatorname{erfc}\left(\frac{x}{2}\right) \exp\left(-\frac{x}{\zeta_2\sqrt{\overline{\gamma}_{RRF}}\mathcal{NB}}\right) dx. \tag{27}$$

Rearranging Eq. (27) and using Eq. (2.8.5-2) of [26], we finally have

$$BER_{RRF} = \frac{2^{\zeta_1}}{\sqrt{\pi}\left(\zeta_2\sqrt{\overline{\gamma}_{RRF}}\mathcal{NB}\right)^{\zeta_1+1}\Gamma(\zeta_1+1)} \times \left\{\frac{\Gamma\left(\frac{\zeta_1+2}{2}\right)}{\zeta_1+1} {}_2F_2\left(\mathfrak{a}-\frac{1}{2}, \mathfrak{b}-\frac{1}{2}; \mathfrak{c}-\frac{1}{2}, \mathfrak{d}-1; \mathfrak{e}\right) - \frac{2\Gamma\left(\frac{\zeta_1+3}{2}\right)}{(\zeta_1+2)\,\zeta_2\sqrt{\overline{\gamma}_{RRF}}\mathcal{NB}} {}_2F_2(\mathfrak{a}, \mathfrak{b}; \mathfrak{c}, \mathfrak{d}; \mathfrak{e})\right\}, \tag{28}$$

where $\mathfrak{a} = \frac{\zeta_1+2}{2}$, $\mathfrak{b} = \frac{\zeta_1+3}{2}$, $\mathfrak{c} = \frac{\zeta_1+4}{2}$, $\mathfrak{d} = \frac{3}{2}$, and $\mathfrak{e} = \left(\zeta_2\sqrt{\overline{\gamma}_{RRF}}\mathcal{NB}\right)^{-2}$.

B. Outage Probability

Inserting the PDF of the RIS-assisted RF channel given in Eq. (25) into Eq. (7), the CDF will be as

$$F_{\gamma_{RRF}}(\gamma_{RRF}) = \frac{1}{2\left(\zeta_2\sqrt{\overline{\gamma}_{RRF}}\mathcal{NB}\right)^{\zeta_1+1}\Gamma(\zeta_1+1)} \times \int_0^{\gamma_{RRF}} x^{\frac{\zeta_1-1}{2}} \exp\left(-\frac{\sqrt{x}}{\zeta_2\sqrt{\overline{\gamma}_{RRF}}\mathcal{NB}}\right) dx. \tag{29}$$

Rearranging Eq. (29), and posing the following variable transformation *i.e.*, $\sqrt{x} = t$, we have

$$F_{\gamma_{RRF}}(\gamma_{RRF}) = \frac{1}{\left(\zeta_2\sqrt{\overline{\gamma}_{RRF}}\mathcal{NB}\right)^{\zeta_1+1}\Gamma(\zeta_1+1)} \times \int_0^{\sqrt{\gamma_{RRF}}} t^{\zeta_1} \exp\left(-\frac{t}{\zeta_2\sqrt{\overline{\gamma}_{RRF}}\mathcal{NB}}\right) dt. \tag{30}$$

Then, applying Eq. (2.3.6-1) from [27] into Eq. (29) we obtain

$$F_{\gamma_{RRF}}(\gamma_{RRF}) = \frac{\left(\sqrt{\gamma_{RRF}/\overline{\gamma}_{RRF}}\right)^{\zeta_1+1}}{\left(\zeta_2\mathcal{NB}\right)^{\zeta_1+1}(\zeta_1+1)\Gamma(\zeta_1+1)} \times {}_1F_1\left(\zeta_1+1; \zeta_1+2; -\frac{\sqrt{\gamma_{RRF}}}{\zeta_2\sqrt{\overline{\gamma}_{RRF}}\mathcal{NB}}\right). \tag{31}$$

Finally, using the definition of OP in Eq. (9), the OP becomes

$$P_{out,RRF} = \frac{\left(\sqrt{\gamma_{RRF_{th}}/\overline{\gamma}_{RRF}}\right)^{\zeta_1+1}}{\left(\zeta_2\mathcal{NB}\right)^{\zeta_1+1}(\zeta_1+1)\Gamma(\zeta_1+1)} \times {}_1F_1\left(\zeta_1+1; \zeta_1+2; -\frac{\sqrt{\gamma_{RRF_{th}}/\overline{\gamma}_{RRF}}}{\zeta_2\mathcal{NB}}\right). \tag{32}$$

C. Channel Capacity

The channel capacity can be expressed as in Eq. (11) considering γ_{RRF}. By inserting the PDF of the SNR given in Eq. (25), we then obtain the following expression of the RRF channel capacity *i.e.*,

$$C_{RRF} = \frac{1}{\ln 2}\int_0^\infty \frac{\ln(1+\gamma_{RRF})\,\gamma_{RRF}^{\frac{\zeta_1-1}{2}}}{2\left(\zeta_2\sqrt{\overline{\gamma}_{RRF}}\mathcal{NB}\right)^{\zeta_1+1}\Gamma(\zeta_1+1)} \tag{33}$$

$$\times \exp\left(-\frac{\sqrt{\gamma_{RRF}}}{\zeta_2\sqrt{\overline{\gamma}_{RRF}}\mathcal{NB}}\right) d\gamma_{RRF}. \tag{34}$$

Since we can express the logarithmic and exponential functions respectively as

$$e^{-x} = G_{0,1}^{1,0}\left(x\middle|\begin{matrix}-\\0\end{matrix}\right), \quad \ln(1+x) = G_{2,2}^{1,2}\left(x\middle|\begin{matrix}1,1\\1,0\end{matrix}\right), \tag{35}$$

then, Eq. (33) becomes

$$C_{RRF} = \frac{\left(\zeta_2\sqrt{\overline{\gamma}_{RRF}}\mathcal{NB}\right)^{-(\zeta_1+1)}}{2\ln(2)\Gamma(\zeta_1+1)}\int_0^\infty d\gamma_{RRF}\gamma_{RRF}^{\frac{\zeta_1-1}{2}} \times G_{2,2}^{1,2}\left(\gamma_{RRF}\middle|\begin{matrix}1,1\\1,0\end{matrix}\right) G_{0,1}^{1,0}\left(\frac{\sqrt{\gamma_{RRF}}}{\zeta_2\sqrt{\overline{\gamma}_{RRF}}\mathcal{NB}}\middle|\begin{matrix}-\\0\end{matrix}\right). \tag{36}$$

Finally, applying [21, Eq. (07.34.21.0013.01)], we obtain

$$C_{RRF} = \frac{2^{\zeta_1}}{\sqrt{\pi}\ln(2)\Gamma(\zeta_1+1)} \times G_{2,4}^{4,1}\left(\left(\frac{1}{2\zeta_2\sqrt{\overline{\gamma}_{RRF}}\mathcal{NB}}\right)^2\middle|\begin{matrix}0,1\\\frac{\zeta_1+1}{2}, \frac{\zeta_1+2}{2}, 0, 0\end{matrix}\right). \tag{37}$$

VI. Asymptotic Analysis

This section delves into the asymptotic analysis of the average BER, the OP, and the channel capacity in high SNR regimes, and examines the diversity order.

A. Average BER

Using Eqs. (2.9.15), (1.5.9) and (1.5.10) from [28], the BER of RF LoS link given in Eq. (6) approximates to

$$\underset{\overline{\gamma}_{RF}\gg 1}{BER_{RF}} = \frac{\Gamma(m+1/2)(4m)^{m-1/2}}{\Gamma(m)\sqrt{\pi m}\Omega^m}\overline{\gamma}_{RF}^{-m}, \tag{38}$$

for its big arguments resulting from high SNR condition. Then, the diversity order for BER of RF LoS link is $\mathcal{O}_{BER}^{RF} = m$.

For RIS-assisted RF link, applying Eq.(07.32.03.0001.01) from [21] for the generalized hypergeometric function to the BER given in Eq. (28), the asymptotic expansion of the average BER for high SNR can be obtained by

$$\underset{\overline{\gamma}_{RRF}\gg 1}{BER_{RRF}} = \mathcal{B}_a\overline{\gamma}_{RRF}^{-\frac{\zeta_1+1}{2}} - \mathcal{B}_b\overline{\gamma}_{RRF}^{-\frac{\zeta_1+2}{2}}, \tag{39}$$

where $\mathcal{B}_a = \mathcal{N}^{-(\zeta_1+1)}\mathcal{B}_x$, $\mathcal{B}_b = \mathcal{N}^{-(\zeta_1+2)}\mathcal{B}_y$ and, $\mathcal{B}_x$ and $\mathcal{B}_y$ are respectively

$$\mathcal{B}_x = \frac{2^{\zeta_1}\Gamma\left(\frac{\zeta_1+2}{2}\right)}{\pi(\zeta_1+1)\left(\zeta_2\mathcal{B}\right)^{\zeta_1+1}\Gamma(\zeta_1+1)\Gamma\left(\frac{\zeta_1+3}{2}\right)}, \tag{40}$$

$$\mathcal{B}_y = \frac{2^{\zeta_1+2}\Gamma\left(\frac{\zeta_1+3}{2}\right)}{\pi(\zeta_1+2)\left(\zeta_2\mathcal{B}\right)^{\zeta_1+2}\Gamma(\zeta_1+1)\Gamma\left(\frac{\zeta_1+4}{2}\right)}. \tag{41}$$

It can be seen that $\mathcal{B}_a$ and $\mathcal{B}_b$ are independent from the average SNR. From Eq. (39), the contribution of terms to the diversity is with the orders of $\frac{\zeta_1+1}{2}$ and $\frac{\zeta_1+2}{2}$, respectively. Then, the diversity order can be defined as

$$\mathcal{O}_{BER}^{RRF} = \min\left[(\zeta_1+1)/2, (\zeta_1+2)/2\right], \tag{42}$$

and since $\zeta_1 > 0$, Eq. (42) becomes $\mathcal{O}_{BER}^{RRF} = (\zeta_1+1)/2$. Finally, for high number of RIS elements, Eqs. (39) can be revised as

$$\underset{\mathcal{N}\gg 1}{BER_{RRF}} = \mathcal{B}_c\mathcal{N}^{-(\zeta_1+1)} - \mathcal{B}_d\mathcal{N}^{-(\zeta_1+2)}, \tag{43}$$

where $\mathcal{B}_c = \overline{\gamma}_{RRF}^{-\frac{\zeta_1+1}{2}}\mathcal{B}_x$, $\mathcal{B}_d = \overline{\gamma}_{RRF}^{-\frac{\zeta_1+2}{2}}\mathcal{B}_y$. Then, the diversity order for the BER of RIS assisted RF link for high number of RIS elements becomes $\mathcal{O}_{BER}^{RRF} = \zeta_1 + 1$.

B. Outage Probability

Using Eq. (06.06.06.0002.01) from [21], the asymptotic expression for OP of RF link given in Eq. (10) becomes

$$\underset{\overline{\gamma}_{RF}\gg 1}{P_{out,RF}} = \sum_{n=0}^{\infty}\frac{(-1)^n\left(m\gamma_{RF_{th}}\right)^{m+n}}{n!(m+n)\Omega^{m+n}}\overline{\gamma}_{RF}^{-(m+n)}. \tag{44}$$

It is seen that the series expansion in Eq. (44) is dominated by the first term when $n = 0$, and then the diversity order becomes $\mathcal{O}_{P_{out}}^{RF} = m$. According to [29, pp.75], the hypergeometric function ${}_1F_1\left(a;c;-x\right)$ can be approximated for its small argument by ${}_1F_1\left(a;c;-x\right) \approx 1-(a/c)\,x$, when $x \ll 1$. Applying such approximation to Eq. (32), the outage probability can be approximated in high SNR regime by

$$\underset{\overline{\gamma}_{RRF}\gg 1}{P_{out,RRF}} = \mathcal{B}_e\overline{\gamma}_{RRF}^{-\frac{\zeta_1+1}{2}} - \mathcal{B}_f\overline{\gamma}_{RRF}^{-\frac{\zeta_1+2}{2}}, \tag{45}$$

where $\mathcal{B}_e = \mathcal{N}^{-(\zeta_1+1)}\mathcal{B}_s$, $\mathcal{B}_f = \mathcal{N}^{-(\zeta_1+2)}\mathcal{B}_t$ and, $\mathcal{B}_s$ and $\mathcal{B}_t$ are respectively given as

$$\mathcal{B}_s = \gamma_{RRF_{th}}^{\frac{\zeta_1+1}{2}}/\left[(\zeta_1+1)\left(\zeta_2\mathcal{B}\right)^{\zeta_1+1}\Gamma(\zeta_1+1)\right], \tag{46}$$

$$\mathcal{B}_t = \gamma_{RRF_{th}}^{\frac{\zeta_1+2}{2}}/\left[(\zeta_1+2)\left(\zeta_2\mathcal{B}\right)^{\zeta_1+2}\Gamma(\zeta_1+1)\right]. \tag{47}$$

Using a similar approach given in Eq. (42), the diversity order for the OP can be found as $\mathcal{O}_{P_{out}}^{RRF} = (\zeta_1+1)/2$. Finally, for high number of RIS elements, Eq. (42) can be rearranged as

$$\underset{\mathcal{N}\gg 1}{P_{out,RRF}} = \mathcal{B}_g\mathcal{N}^{-(\zeta_1+1)} - \mathcal{B}_h\mathcal{N}^{-(\zeta_1+2)}, \tag{48}$$

where $\mathcal{B}_g = \overline{\gamma}_{RRF}^{-\frac{\zeta_1+1}{2}}\mathcal{B}_s$ and $\mathcal{B}_h = \overline{\gamma}_{RRF}^{-\frac{\zeta_1+2}{2}}\mathcal{B}_t$. Then, the first term in Eq. (48) will be the diversity order as $\mathcal{O}_{P_{out}}^{RRF} = \zeta_1 + 1$.

C. Channel Capacity

Assuming that $\gamma_{RF} \gg 1$, Eq. (11) can be written as

$$\underset{\overline{\gamma}_{RF}\gg 1}{C_{RF}} = \frac{1}{\ln(2)}\int_0^{\infty}\ln\left(\gamma_{RF}\right)f_{\gamma_{RF}}(\gamma_{RF})d\gamma_{RF}. \tag{49}$$

Applying Eq.(2.6.21.2) from [27], the channel capacity of RF link can be expressed as

$$\underset{\overline{\gamma}_{RF}\gg 1}{C_{RF}} = \frac{1}{\ln(2)}\left[\psi(m) - \ln\left(m/(\overline{\gamma}_{RF}\Omega)\right)\right]. \tag{50}$$

where $\psi(\cdot)$ denotes the Digamma (psi) function. Considering the expression of γ_{RRF} in Eq. (26), the ergodic channel capacity in high SNR regime can be written as

$$\underset{\overline{\gamma}_{RRF}\gg 1}{C_{RRF}} = \frac{\left(\zeta_2\sqrt{\overline{\gamma}_{RRF}}\mathcal{N}\mathcal{B}\right)^{-(\zeta_1+1)}}{2\ln(2)\Gamma\left(\zeta_1+1\right)}\int_0^{\infty}d\gamma_{RRF} \times\gamma_{RRF}^{\frac{\zeta_1-1}{2}}\ln\left(\gamma_{RRF}\right)\exp\left(-\frac{\sqrt{\gamma_{RRF}}}{\zeta_2\sqrt{\overline{\gamma}_{RRF}}\mathcal{N}\mathcal{B}}\right). \tag{51}$$

Then, applying Eq.(2.6.21.2) of [27] to Eq. (51), the ergodic capacity in high SNR regime is found to be

$$\underset{\overline{\gamma}_{RRF}\gg 1}{C_{RRF}} = \frac{2\left[\psi(\zeta_1+1) + \ln\left(\mathcal{N}\sqrt{\overline{\gamma}_{RRF}}\right) + \ln\left(\zeta_2\mathcal{B}\right)\right]}{\ln\left(2\right)}. \tag{52}$$

VII. Handover Decision Approach

This section presents our proposed algorithm for handover management in an overlapping network scenario, as depicted in Fig. 1. We assume the UE is the receiving node for an end-to-end communication link, where the source node can be either the BS or the satellite. For simplicity, we call both of them as APs. Algorithm 1 represents the proposed RIS-aided handover technique and investigates how to optimally select a path/single link[1] among multiple available choices in

[1]We assume a path as a NLoS link through the RIS module, while a single link is intended as a direct link to the UE.

case of link failure. The handover decision is taken based on different BER path/single link measurements, and selecting those path/ single link showing better performance. As a result, the proposed approach computes the handover probability both in case of hard and soft modes. Our proposed approach highlights different conditions where the use of RIS-embedded devices are preferred to traditional no-RIS handovers. Let us assume that the UE is in position $P_{UE} = (x, y, z)$ and is connected to a given AP via a LoS connectivity link *i.e.*, l_s, and the associated BER is below a given quality of service (QoS) threshold *i.e.*, 10^{-3}. The connectivity link is monitored at fixed time interval in order to keep the corresponding QoS level acceptable. As soon as the UE is experiencing a BER level from the serving AP higher than a given threshold, the UE will be listening for other available APs for possible connectivity switching. Specifically, we distinguish direct links from no direct ones. A pool of all the available direct links sensed by the UE at position P_{UE} is then built, *i.e.*,

$$\mathcal{L}_{dir}^{(P_{UE})} = \{l_{d,1}, l_{d,2}, \ldots, l_{d,i}, \ldots, l_{d,N}\}, \tag{53}$$

whose corresponding BERs are computed at the UE and are higher than the UE's sensitivity.

In case of decreasing performance of the serving LoS link l_s, it is preferred to maintain the connectivity to the serving AP and switch to NLoS RIS-aided link if available. In this way, the transmitting node will be still the same AP but the connectivity path will change. As a result, no traffic overhead occurs for UE's authentication and association, and the serving AP is still the same except relying on a RIS-aided link. However, in some cases it is preferable to connect to another AP if the achievable performance outperforms the current connectivity link. It follows that we can define the following set of NLoS links through RIS *i.e.*,

$$\mathcal{L}_{nodir}^{(P_{UE})} = \{l_{nd,1}, l_{nd,2}, \ldots, l_{nd,j}, \ldots l_{nd,M}\}, \tag{54}$$

where $l_{nd,j}$ represents the j-th no-direct RIS-aided link.

The **hard handover probability** is defined as the probability to initiate a hard handover from the serving AP associated to link l_s to a candidate one through the i-th link from the set $\mathcal{L}_{dir}^{(P_{UE})}$, based on the average BER measurements *i.e.*,

$$\mathcal{P}_{HHO,l_i} = \Pr\{BER_{l_s} \geqslant Th_h \bigcup BER_{l_i} < BER_{l_s}\}, \tag{55}$$

where BER_{l_s} and BER_{l_i} are the average BER measurements from the serving AP and the i-th link from set $\mathcal{L}_{dir}^{(P_{UE})}$. Of course, the hard handover probability occurs assuming that $BER_{l_i} \leqslant Th_h$, with Th_h as the hard handover threshold, usually set to 10^{-3}. A hard handover is then executed towards that link exhibiting the highest hard handover probability *i.e.*,

$$\max_{i \in \mathcal{L}_{dir}^{(P_{UE})}} \mathcal{P}_{HHO,\mathcal{L}_{dir}^{(P_{UE})}}. \tag{56}$$

Similar to the hard handover case, the **soft handover probability** is defined as the probability to initiate a soft handover from a serving AP associated to link l_s to a candidate one through the i-th link *i.e.*,

$$\mathcal{P}_{SHO,l_i} = \Pr\{Th_s \leqslant BER_{l_s} < Th_h \bigcup BER_{l_i} < Th_s\}, \tag{57}$$

Algorithm 1 RIS-Aided Algorithm for Ground-Aerial-Space Connectivity

Input :
$P_{UE} = (x, y, z)$ ▷ UE's position
$\mathcal{L}_{dir}^{(P_{UE})} = \{l_{d,1}, \ldots, l_{d,i}, \ldots, l_{d,N}\}$ ▷ Set of available direct links
$\mathcal{L}_{nodir}^{(P_{UE})} = \{l_{nd,1}, \ldots, l_{nd,j}, \ldots, l_{nd,M}\}$
▷ Set of available no-direct links
Th_h ▷ Hard HO threshold
Th_s with $Th_s < Th_h$ ▷ Soft HO threshold
$l_s \notin \mathcal{L}_{dir}, \mathcal{L}_{nodir}$ ▷ Serving link
ρ_{l_s} ▷ Active connections served by l_s
λ ▷ Threshold on the number of active connections

Output:
$h = \{HHO, SHO, RIS\text{-}CB, RIS\text{-}PP\}$ ▷ Handover execution

if $BER_{l_s} \geqslant Th_h$ **then**
  forall the $i \in \{1, \ldots, N\}$ **do**
    if $BER_{l_i} < BER_{l_s} \wedge BER_{l_i} \leqslant Th_h$ **then**
      $h \leftarrow HHO$ ▷ Hard handover
if $Th_s < BER_{l_s} \leqslant Th_h$ **then**
  forall the $i \in \{1, \ldots, N\}$ **do**
    if $BER_{l_i} < Th_s$ **then**
      $h \leftarrow SHO$ ▷ Soft handover
if $Th_h - \varepsilon < BER_{l_S} \leqslant Th_h + \varepsilon$ **then**
  forall the $j \in \{1, \ldots, M\}$ **do**
    if $BER_{l_j} < Th$ ▷ *Ping-pong effect* **then**
      $h \leftarrow RIS\text{-}PP$ ▷ RIS-based PP avoidance handover
if $\rho_{l_s} > \lambda$ ▷ *Cell breathing* **then**
  forall the $j \in \{1, \ldots, M\}$ **do**
    if $BER_{l_j} < Th$ **then**
      $h \leftarrow RIS\text{-}CB$ ▷ RIS-based CB handover

where Th_s is the soft handover threshold, with $Th_s < Th_h$. In this case, since the performance of the serving AP is better than the case of hard handover (*i.e.*, $BER_{l_s} < Th_h$), the link from the serving AP will be maintained and the UE will be receiving data from both the serving AP and the candidate one. Similar to previous case, a soft handover will be executed towards that link exhibiting the highest soft handover probability *i.e.*,

$$\max_{i \in \mathcal{L}_{dir}^{(P_{UE})}} \mathcal{P}_{SHO,\mathcal{L}_{dir}^{(P_{UE})}}. \tag{58}$$

Eq. (55) and (57) refer respectively to the traditional hard and soft handover procedure, which involves direct links from different APs. We are now interested in understanding what are those conditions where the use of RIS better works for handover management, w.r.t. the traditional procedure. We then extend the range of applicability of Eq. (55) and (57) to

both $\mathcal{L}_{dir}^{(P_{UE})}$ and $\mathcal{L}_{nodir}^{(P_{UE})}$. Furthermore, exploiting the RIS for handover management allows to define the following handover probabilities where RISs mainly act as coverage extenders, while keeping the same active connection to the serving AP. Specifically, we identify two conditions where RISs are expected to be exploited for handover management *i.e.*, (*i*) cell breathing [30], [31], and (*ii*) ping-pong effect [32], [33].

Cell breathing (CB) is a well-known technique adopted in cellular networks that allows to reduce the traffic load in case it exceeds a given threshold, by accordingly reducing the cell coverage. As a result, users on the borderline of a wireless cell are forced to be connected to another AP. Leveraging on such approach, we define the following **RIS-based CB handover probability** from a serving AP to the j-th no-direct link in the set $\mathcal{L}_{nodir}^{(P_{UE})}$ *i.e.*,

$$\mathcal{P}_{RIS,l_j}^{CB} = \Pr\{\rho_{l_s} > \lambda \bigcup BER_{l_j} < Th_h\}, \tag{59}$$

where ρ_{l_s} is the number of active connections in the serving AP and λ is the threshold (in percentage) that triggers the cell breathing mechanism. Eq. (59) monitors both the traffic load of the serving AP, as well as the average BER from the j-th no-direct link. If the current traffic load exceeds a given threshold *i.e.*, $\rho_{l_s} > \lambda$, and the performance of the j-th link is acceptable *i.e.*, $BER_{l_j} < Th_h$, a handover will be executed to the j-th link. Notice that the j-th link represents a NLoS link from the same serving AP. In this way, the serving AP will be maintained but the signal propagation will be according to the j-th NLoS link exhibiting acceptable performance. Of course, the selection of the j-th link for handover execution will be according to the computation of the maximum handover probability in the set $\mathcal{L}_{nodir}^{(P_{UE})}$. Finally, the *ping-pong (PP) condition* is another situation that can be well supported by the use of RIS. This is a bad condition that causes unwanted and unnecessary handovers, due to fast switching connectivity from two overlapping neighboring wireless networks. In order to avoid such bad situation, the use of RIS allows the UE to maintain the connectivity from the serving AP but relying on RIS-based NLoS link. The following **RIS-based ping-pong avoidance handover probability** is defined as:

$$\begin{aligned}\mathcal{P}_{RIS,l_j}^{PP} = \Pr\{&Th_h - \varepsilon < BER_{l_s} < Th_h + \varepsilon \\ &\bigcup Th_h - \varepsilon < BER_{l_i} < Th_h + \varepsilon \\ &\bigcup BER_{l_j} < Th_h\},\end{aligned} \tag{60}$$

which considers to switch from the serving direct link l_s to the j-th RIS-based NLoS link, if both the BER from l_s and l_i vary in the range $Th_h \pm \varepsilon$, with ε as small as possible, while the BER from the j-th link is lower than the hard handover threshold. As a result, an handover will be executed to the j-th link exhibiting the highest probability according to Eq. (60). Notice that also for the RIS-based ping-pong avoidance handover probability, the serving AP will be maintained through a NLoS RIS-based link. This aspect represents the main feature of RIS-aided handover procedure, which forces to keep the serving AP but redirect the signal propagation through other links.

TABLE I
LIST OF PARAMETERS OF (SINGLE/DOUBLE) NAKAGAMI-m DISTRIBUTION USED IN DIFFERENT USE CASES

Link	**CASE 1A** ($\Omega = 2$)	**CASE 2A** ($m = 2$)
BS1-UE	$m = 1$	$\Omega = 1$
BS2-UE	$m = 1.2$	$\Omega = 1.2$
BS-HAPS-UE	$m_1 = m_2 = 2$	$\Omega_1 = \Omega_2 = 2$
SAT-UE	$m = 3$	$\Omega = 3$
SAT-HAPS-UE	$m_1 = 3; = m_2 = 2$	$\Omega_1 = 3, \Omega_2 = 2$
Link	**CASE 1B** ($\Omega = 2$)	**CASE 2B** ($m = 2$)
BS1-UE	$m = 1.5$	$\Omega = 1.5$
BS2-UE	$m = 1.9$	$\Omega = 1.9$
BS-HAPS-UE	$m_1 = m_2 = 2.4$	$\Omega_1 = \Omega_2 = 2.4$
SAT-UE	$m = 3$	$\Omega = 4$
SAT-HAPS-UE	$m_1 = 3, m_2 = 2.4$	$\Omega_1 = 4, \Omega_2 = 2.4$

VIII. NUMERICAL RESULTS

This section presents MC simulations with 10^8 realizations for the BER, OP, and channel capacity (see Subsection VIII-A), as well as the handover probability (see Subsection VIII-B) for various link configurations and different parameters. For comparison purpose, we also considered (*i*) no-direct links with HAPS acting as a relay node, assuming $\beta = 1$, as well as (*ii*) the traditional handover procedure involving direct links, as depicted in Fig. 2. We also assumed geostationary orbit (GEO) satellites, for which the Doppler shift effect is negligible [34]. The Nakagami-m distribution applies for satellite links as well since, supported by measurement data, it is very likely to model various satellite channels, [35].

Unless specified in either plots or figure captions, parameters are set to $f = 1200\,\text{MHz}$, $\mathcal{N} = [2, 4, 8, 16]$, $\beta = 0.8$, and $\gamma_{th} = 2\,\text{dB}$. In order to better assess the link performance of various links, we consider four different use-cases with variable Ω and m values, as reported in Table I. The values of the parameters m and Ω are chosen by taking into account the fading severity, LoS, and distance of each link configuration. Indeed, the parameter m ranging in $0.5 \leqslant m < \infty$ controls the severity of the fading, so increasing the value of m decreases the severity of fading, and vice versa [36]. Notice that in case of direct LoS links, we consider m and Ω, while for no-direct NLoS paths we have m_1 and m_2 for the first and second link, respectively. In CASE 1A and 2A we consider smaller values of m and Ω, so representing worst conditions, while for CASE 1B and 2B showing higher values of m and Ω it is represented a better scenario. Finally, in Table I for sake of easier reading, BS refers to BS1.

A. BER, OP, and Channel Capacity

In this subsection, we report the behavior of the average BER, the OP, and the capacity achieved for different direct and no-direct connectivity links, for different cases. MC simulations and asymptotic analysis in case of high SNR are also depicted in order to assess the theoretical trends. In the next figures, MC simulations and the asymptotic analysis are reported as circle purple and square magenta markers, respectively.

As a first insight of Fig. 3(*a*), we observe that for increasing number of RIS elements the average BER decreases. On the

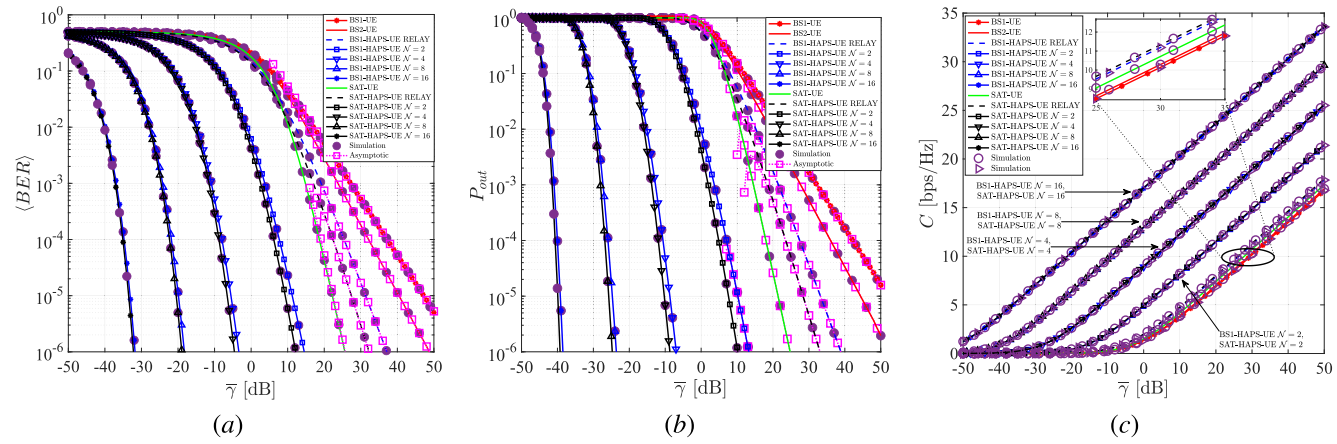

Fig. 3. CASE 1A. Performance comparison *i.e.*, (*a*) average BER variation, (*b*) OP, and (*c*) link capacity, versus the average SNR, for different direct and HAPS-assisted link configurations.

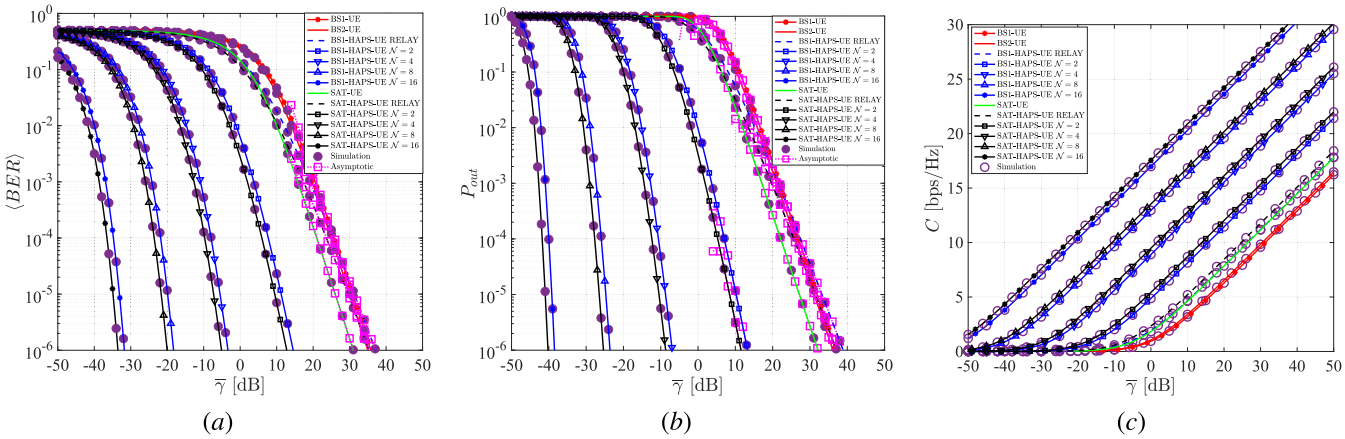

Fig. 4. CASE 2A. Performance comparison *i.e.*, (*a*) average BER variation, (*b*) OP, and (*c*) link capacity, versus average SNR, for different direct and HAPS-assisted link configurations.

other side, in case of direct links, performance is slowly improving for higher values of average SNR. Worst results are obtained for the direct ground links observing a small benefit with lower value of m. Interesting, the satellite direct link presents better performance than the no-direct SAT-HAPS-UE link in case of relay node (see dashed black curve). However, for no-direct SAT-HAPS-UE links with RIS, performances are improved, showing a quick decreasing slope for high number of RIS elements. This implies that, the benefit of RIS-aided link can be seen more when the number of RIS elements increases. From Fig. 3, comparing no-direct satellite and ground links (*i.e.*, black and blue curves) we observe an almost overlapping trend for high number of RIS elements, while for smaller values of $\mathcal{N}$ a performance gap is observed, showing better performance in case of no-direct satellite links. The superiority of SAT-HAPS-UE link is due to the values of m and Ω, which show higher values thus reducing fading. A similar behavior is observed from the results given for the OP in Fig. 3(*b*). Specifically, increasing values of $\mathcal{N}$ allows to reach higher performance, as also depicted in Fig. 3(*c*) for the channel capacity. However, in this latter case, we observe very close overlapping curves for both no-direct satellite and ground links. At the same time, we can appreciate the capacity gain with the use of RIS versus direct links, as well as no-direct relay-based links. Due to the overlapping of different curves, in Fig. 3(*c*) we use circle and triangle purple markers in order to improve the readiness of the plots. Since the asymptotic results perfectly match the analytical ones, we omitted them.

Using the parameters of CASE 2A, the variations of average BER, OP, and channel capacity are shown in Fig. 4. As it is observed in Fig. 3, the performance improvement with the increase of the parameter m is seen. The reason for this performance improvement is the reduction of the severity of fading with the increase of m. The benefit of using higher number of RIS and the superiority of the SAT-HAPS-UE is also observed from Fig. 4.

The effect of parameter Ω together with the RIS application on the average BER, OP and channel capacity of different link configurations is illustrated in both Fig. 5 and Fig. 6. While the performance of links enhances with the increase of average power Ω, the performance improvement multiplies when the effect of average power is combined with the increased number of RIS. SAT-HAPS-UE and BS-HAPS-UE links with the same number of reflecting elements $\mathcal{N} = 4$ yield the best performances, respectively. The performance of direct links (*e.g.*, BS-UE or SAT-UE) can dominate the performance of HAPS-assisted links only when the number of RIS elements is fixed to $\mathcal{N} = 1$. Finally, Fig. 7 depicts the BER performance

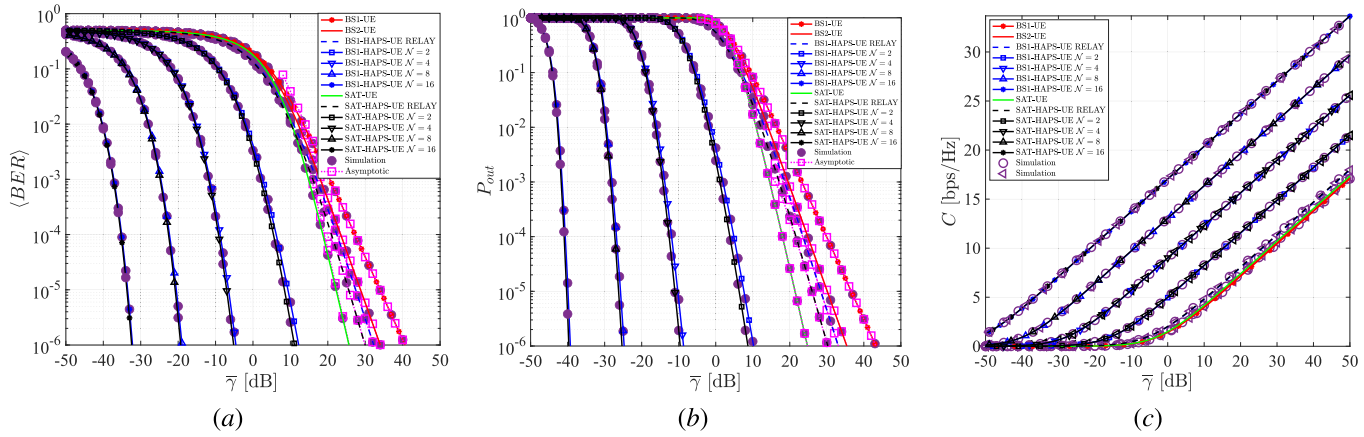

Fig. 5. CASE 1B. Performance comparison *i.e.*, (*a*) average BER variation, (*b*) OP, and (*c*) link capacity, versus average SNR, for different direct and HAPS-assisted link configurations.

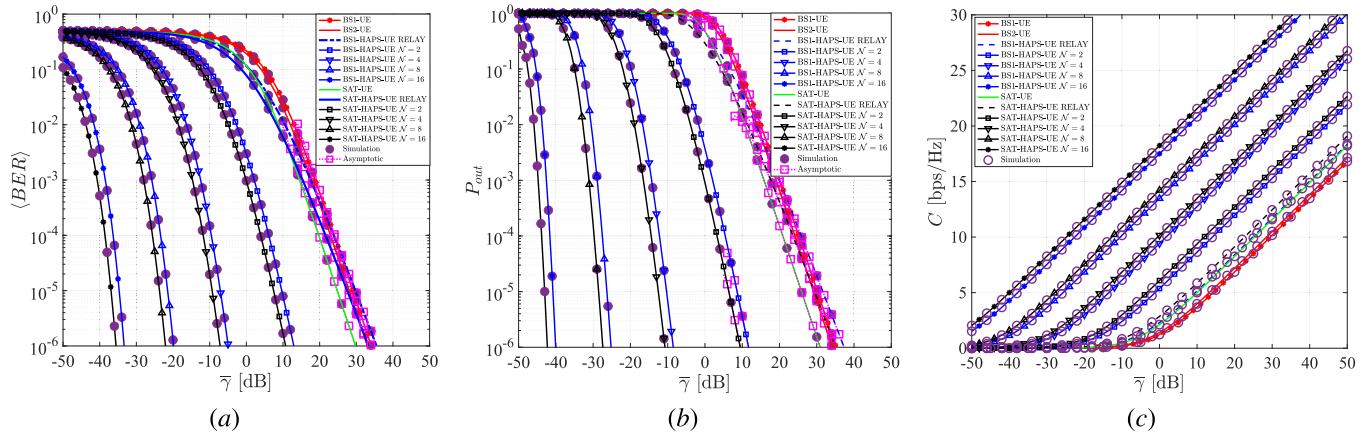

Fig. 6. CASE 2B. Performance comparison *i.e.*, (*a*) average BER variation, (*b*) OP, and (*c*) link capacity, versus average SNR, for different direct and HAPS-assisted link configurations.

in case of no-direct ground and satellite links with variable number of RIS elements, achieved for CASE 1A. As expected, for increasing number of RIS elements the link performances increase. A higher behavior is observed for no-direct BS-HAPS-UE links, but an overlapping trend is achieved for channel capacity. Indeed, as also observed in previous Fig. 3-6 the link capacity presents small variations for different curves, and an overlapping behavior specially for increasing number of RIS elements. Also in this case, we observe the good match between analytical and MC simulations.

B. Handover Probability

After evaluating the behavior of different wireless links, we are interested in the performance of the proposed handover mechanism, compared to the traditional handover procedure, consisting of link switching from a serving AP to a candidate AP, and also with traditional relay nodes with AF mode.

Fig. 8 depicts the hard handover probability versus the hard handover threshold, computed for direct and no-direct ground and satellite links. For the no-direct links, we assume (*i*) the HAPS is acting as a traditional relay and (*ii*) the HAPS is embedded with a passive RIS with variable number of elements. The hard handover probability shows a decreasing trend for increasing the handover threshold; indeed, if this threshold is high the handover probability will be very small as the handover does not provide a performance gain. The behavior of the hard handover probability is obtained from Eq. (55), which computes the average BER both from the serving link and other available ones. The hard handover probability represents the probability to switch from a serving link to a new one if the BER of the serving link is higher or equal to the hard handover threshold, and also if the BER of a candidate link is lower than that from the serving one.

From Fig. 8(*a*), we observe the highest trends are experienced in case of (*i*) handovers from a direct link to a no-direct RIS-embedded one (see red curves on the top), as well as (*ii*) handover from a no-direct BS-HAPS-UE relay-based link toward a direct link (see black curve with square markers). Indeed, the direct link is always preferred w.r.t. no-direct ones, except when the handover is towards a no-direct link with RIS. The case of traditional hard handover (magenta curves) that consists in connectivity switching from direct BS1 link to BS2, and vice versa, presents the associated handover probabilities lower than those achieved for handover towards no-direct RIS-based links (red curves), thus meaning the benefit of adopting RIS devices for gaining better performance. Reduced values of handover probability are observed when switching from a no-direct relay link to a no-direct RIS-embedded link (see

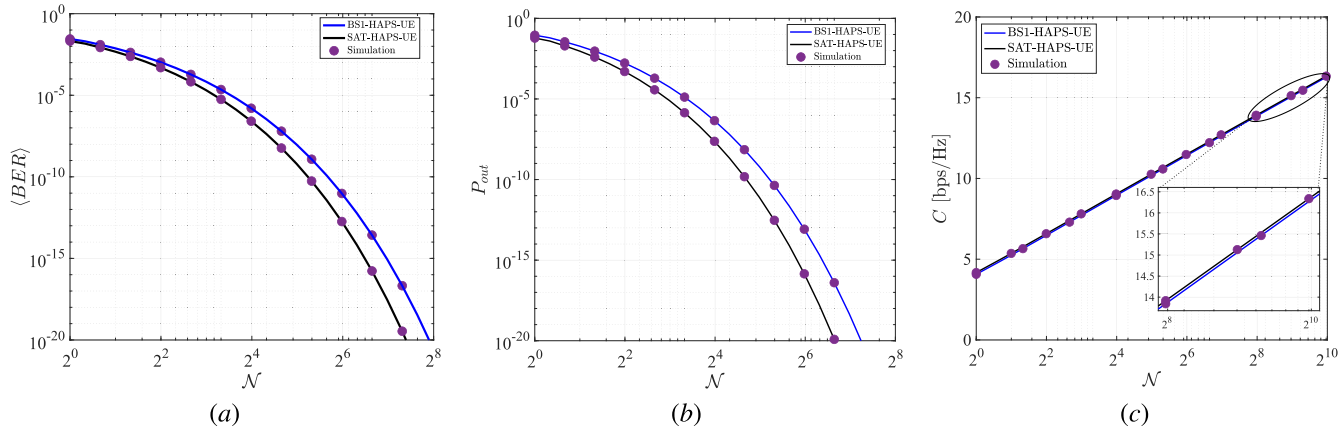

Fig. 7. CASE 1A. Performance comparison of no-direct BS1-HAPS-UE and SAT-HAPS-UE links for (*a*) average BER variation, (*b*) OP, and (*c*) link capacity, versus the number of RIS elements.

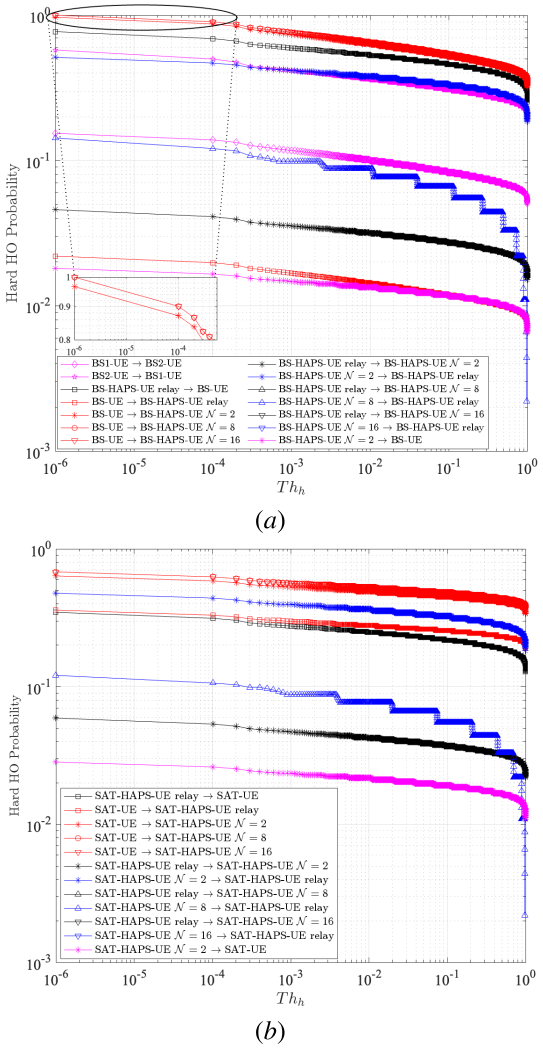

Fig. 8. Hard handover probability versus the handover threshold in case of direct and no direct (*a*) ground and (*b*) satellite links, in case of relay and RIS-embedded links. Markers refer to MC simulations. Parameters for BER computation are from CASE 1A.

black curves). In this case, for increasing number of RIS elements the handover probability is approximated to 0. This is well justified since the gain associated to a RIS-aided link with a higher number of elements is higher than the gain associated to a RIS-aided link with a lower number of elements. It is also interesting to observe a very low (*i.e.*, ≈ 0) handover probability when switching from a no-direct RIS-embedded link to a no-direct relay link, for increasing number of RIS elements. A similar behavior is described in Fig. 8(*b*) in case of hard handover for satellite links, assuming (*i*) no-direct relay and (*ii*) RIS-embedded links. The highest performance are observed in case of hard handover from a direct SAT link to a no-direct RIS-embedded link for $\mathcal{N} = [8, 16]$. This overlapping behavior is due to the high performance achieved for increasing number of RIS elements, as showed in Fig. 7(*a*). Other curves show lower handover probability meaning that there is no particular gain in making a connectivity switching. For instance, moving from a SAT-HAPS-UE relay link to a no-direct SAT-HAPS-UE link embedded with RIS with $\mathcal{N} = 2$ does not provide any significant gain and then the handover probability is very low.

Finally, from Fig. 8 we can observe a perfect match between the analytical and simulation results that validates the accuracy of our approach. One of the reasons for this good match is that the approximations are typically chosen to closely mirror the actual physical and statistical properties of the fading environment. Also, the shape parameter m and the spread parameter Ω are generally estimated from experimental data, making possible the usage of the statistical behaviour of real channel conditions. Another reason relies on the MC simulations that are carried out with large realization numbers and high accuracy, in order to validate the analytical models incorporating almost the same assumptions as the analytical derivations. A similar consideration applies to all the other MC simulation results perfectly matching the analytical ones.

More details on how the handover probability is affected by the number of RIS elements, in case of switching toward a no-direct RIS-embedded link are shown in Fig. 9. The hard handover is computed in case of (*i*) direct ground and no-direct ground-aerial-ground links, and (*ii*) direct satellite and no-direct satellite-aerial-ground links. Specifically, in Fig. 9(*a*) we compare the handover probability from a direct BS-UE link to a BS-HAPS-UE link (see black curves), to the handover

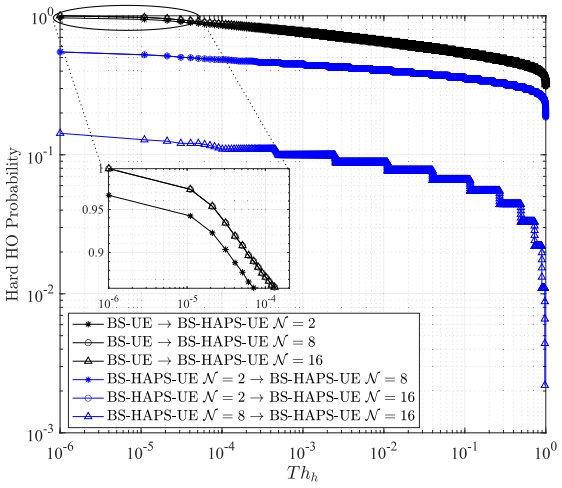

(*a*)

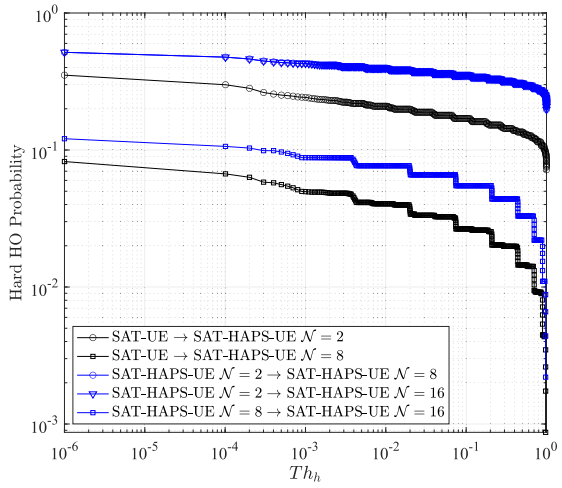

(*b*)

Fig. 9. Hard handover probability versus the handover threshold in case of direct and no direct (*a*) ground and (*b*) satellite links, for different number of RIS elements. Parameters for BER computation are from CASE 1A.

probabilities associated to the switch from BS-HAPS-UE link to another no-direct link with the same technology (see blue curves), with variable RIS elements. We notice that the hard handover probability is maximum for the switch from the direct BS-UE link to the NLoS BS-HAPS-UE link with higher RIS elements. In particular, we observe a small gap for different RIS elements, meaning there is no so much gain for high values of $\mathcal{N}$. Also, lower handover probabilities are experienced in case of switching from a no-direct BS-HAPS-UE link to another BS-HAPS-UE link with variable RIS elements (see blue curves). The lowest trend is in case of switching from a path with RIS $\mathcal{N}=8$ to $\mathcal{N}=16$, while higher values are for switching from a path with $\mathcal{N}=2$ to another with $\mathcal{N}=[8,16]$. Indeed, the gain achieved for the latter case is higher than that in case of switching from $\mathcal{N}=8$ to $\mathcal{N}=16$. A similar consideration can be taken in case of the handover probability associated to the switching from two no-direct links, from $\mathcal{N}=8$ to $\mathcal{N}=16$. In this case, the hard handover probability will be the lowest as the benefit from moving from a link with RIS $\mathcal{N}=8$ to another

TABLE II

COMPARISON OF HANDOVER PROBABILITY FOR DIFFERENT DIRECT AND NO-DIRECT GROUND AND SATELLITE CONNECTIVITY LINKS

From link \ To link	BS2-UE	BS-HAPS-UE with $\mathcal{N}$-elements RIS	BS-HAPS-UE relay
BS1-UE	low	high, increases for high $\mathcal{N}$	very low
BS-HAPS-UE with $\mathcal{N}$-elements RIS	very low	increases for high $\mathcal{N}$	reduces for high $\mathcal{N}$
BS-HAPS-UE relay	high	low, reduces for high RIS	–

From link \ To link	SAT-UE	SAT-HAPS-UE $\mathcal{N}$	SAT-HAPS-UE relay
SAT-UE	–	high, increases for high $\mathcal{N}$	very low
SAT-HAPS-UE with $\mathcal{N}$-elements RIS	very low	increases for high $\mathcal{N}$	reduces for high $\mathcal{N}$
SAT-HAPS-UE relay	high	low, reduces for high RIS	–

link with $\mathcal{N}=16$ is limited as compared to the other link switches.

A different behavior is noticed in Fig. 9(*b*) for the hard handover probability of satellite connectivity. The hard handover probability switching from a direct satellite link to the satellite-aerial-ground (see black curves) is lower than the probability of switching from a no-direct link to another no-direct link with variable RIS number. Indeed, the handover probability will be higher in case of connectivity switching from the link with RIS $\mathcal{N}=2$ to a no-direct link with $\mathcal{N}=[8,16]$. Notice that the overlapping curves in case of switching from a no-direct link to another one with $\mathcal{N}=8$ and $\mathcal{N}=16$ is due since for increasing RIS elements the associated BER performances improve but the handover probability saturates. Smaller values of handover probability are then achieved in case of switching from RIS link with $\mathcal{N}=8$ to $\mathcal{N}=16$. This allows to state that it is preferred to increase the number of RIS elements rather than changing from a direct satellite link to a no-direct satellite-aerial-ground one. For comparison purpose, in Table II we report the qualitative behavior of hard handover probability for different connectivity links. High handover probability means a preferred handover, while low probability refers to a low benefit in performing an handover. The soft handover probability is depicted in Fig. 10. Notice that the soft handover threshold is ranging from 10^{-6} to 10^{-3}, due to more strictly requirements as compared to the hard handover (*i.e.*, $Th_s < Th_h$). It follows that the soft handover probability is smaller than the hard one, and limited to the range of existence of the soft handover threshold. In Fig. 10(*a*) the highest values of the soft handover probability are associated to the switching from a direct BS-UE link to a no-direct RIS-based BS-HAPS-UE link with $\mathcal{N}=16$ (black curve), while lower values are for handovers associated to no-direct BS-HAPS-UE links for different number of RIS elements (blue curves). This is due since the performance of a direct ground link presents the lowest performance as compared to the other connectivity links, and then the associated soft handover probability is higher. On the other side, performance in case of no-direct

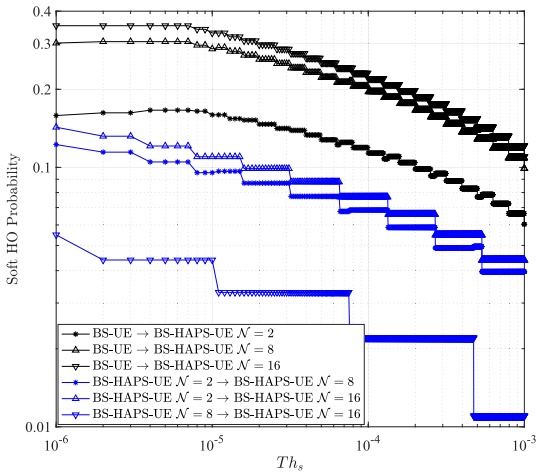

(*a*)

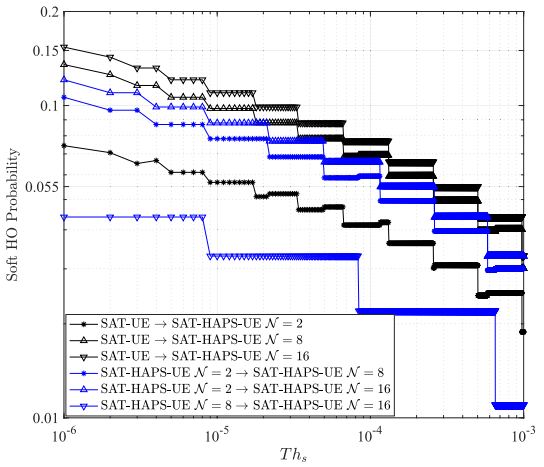

(*b*)

Fig. 10. Soft handover probability versus the handover threshold in case of direct and no direct (*a*) ground and (*b*) satellite links, for different number of RIS elements. Markers refer to MC simulations. The hard handover threshold is set to $Th_h = 0.2$. Parameters for BER computation are from CASE 1A.

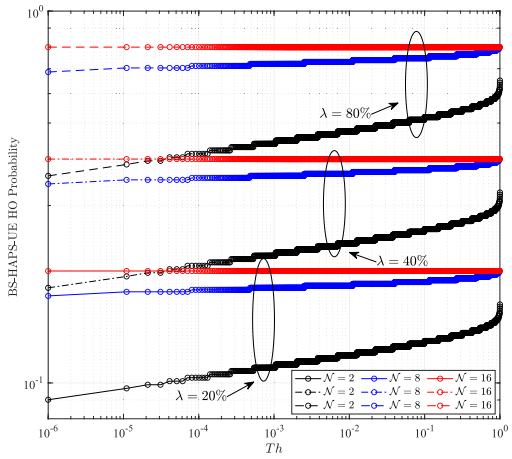

(*a*)

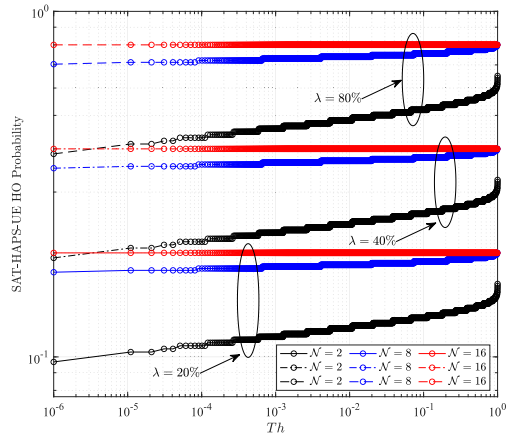

(*b*)

Fig. 11. Handover probability in case of exceeding the network traffic load, from (*a*) BS-UE to BS-HAPS-UE and (*b*) SAT-UE to SAT-HAPS-UE, for different number of RIS elements. Markers refer to MC simulations. Parameters for BER computation are from CASE 1A.

ground-to-aerial-to-ground with the use of RIS is already good, and a soft handover is expected to not enhance so much the overall performance. As a consequence, the associated soft handover probability will be quite small. Also, we evince that a soft handover with no-direct links with higher RIS elements is preferred than the case of links with lower RIS elements. However, if the BER of the serving link is out of the range $[Th_s, Th_h]$ as the performances are much better (*i.e.*, $BER < Th_s$), then the soft handover probability will be reduced. This happens for the soft handover between SAT-HAPS-UE link with $\mathcal{N} = 8$ and SAT-HAPS-UE link with $\mathcal{N} = 16$, whose associated probability is the lowest.

Similar considerations apply to the scenario of satellite connectivity, as depicted in Fig. 10(*b*). Also in this case, the highest performance is associated to the soft handover probability from a direct SAT link to a no-direct RIS-based SAT-HAPS-UE link. However, we notice the associated soft handover probabilities are reduced as compared to Fig. 10(*a*). This is due to the fact that the direct satellite link presents better performance than the ground link, as well as the no-direct RIS-based ground-to-aerial-to-ground links have better behavior (see Fig. 3). Thus, the soft handover probability is expected to be quite small as no particular benefit can be achieved. Furthermore, in this case, the soft handover probability is higher for increasing number of RIS elements, assuming that the performance of each link relies on the soft handover constraints *i.e.*, $Th_s \leqslant BER < Th_h$, as in Eq. (57).

We are now interested in understanding when it is more appropriate to exploit RIS-based links for handover management. In Fig. 11(*a*) we present the handover probability associated to the switch from a direct ground-to-ground link to a ground-to-aerial-to-ground RIS-based one, in case that the traffic load managed by the serving BS is increasing and exceeding a given threshold *i.e.*, λ. We notice that for high percentage of traffic load threshold the handover probability will be higher, while limited values are achieved for a reduced traffic load percentage. This is due since an increase of traffic load can affect the network performance, and then a handover procedure is appropriate to balance the traffic. Furthermore, in line with the previous results, increasing values of handover probability are observed for high values of RIS elements, till reaching a flat behavior when $\mathcal{N} = 16$. Notice also that for high values of handover threshold, the associated probability

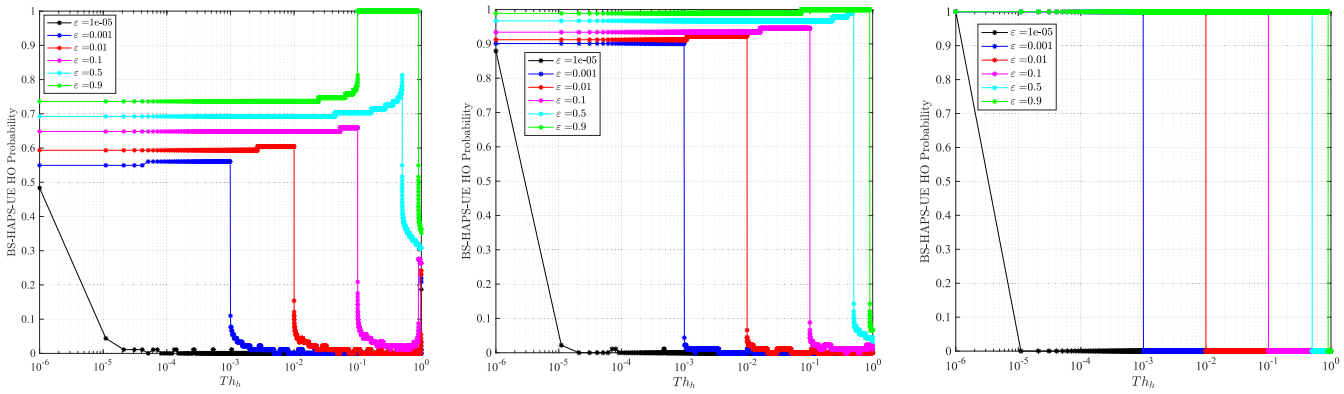

Fig. 12. Handover probability from a direct BS-to-UE link to a no-direct BS-HAPS-UE link with RIS in case of ping-pong effect, for different values of ε and RIS elements *i.e.*, (*a*) $\mathcal{N} = 2$, (*b*) $\mathcal{N} = 5$, and (*c*) $\mathcal{N} = 16$. Markers refer to MC simulations. Parameters for BER computation are from CASE 1A.

increases. A similar behavior is also for SAT links, depicted in Fig. 11(*b*).

Last, Fig. 12 presents the handover probability associated to the switching from a direct ground-to-ground link to a RIS-based ground-to-aerial-to-ground one for different RIS elements, in case of ping-pong effect. As introduced in Eq. (60), ε represents a small variation from the handover threshold that may cause the unwanted ping-pong effect. For increasing values of ε, the handover probability $\mathcal{P}_{RIS}^{PP}$ is higher with a smooth increasing behavior, followed by a fast decreasing slope for high handover threshold. This means that it is preferable to make a handover when the threshold Th_h is lower than a given value, which can be observed to be 10^{-6}, 10^{-3}, and 10^{-2} respectively for $\varepsilon = 10^{-5}$, $\varepsilon = 10^{-4}$, and $\varepsilon = 10^{-3}$, according to the results shown in Fig. 12(*a*). Once overcome this threshold, the handover probability will strongly decrease reaching an almost null value. This behavior is mainly due to the fact that when the handover threshold Th_h increases, the link requirements are easily reached and therefore there will be no need to make a handover.

Interesting, in Fig. 12(*a*), for high handover thresholds (*i.e.*, $Th_h \approx 1$) the handover probability shows small increasing values, till reaching a not null value. For increasing number of RIS elements as depicted in Fig. 12(*b*), the handover probability switches from high (*i.e.*, > 0.9) to low values (*i.e.*, ≈ 0), for different values of ε, till reaching a kind of on-off behavior independently on the ε values in Fig. 12(*c*). This latter trend is due to the high number of RIS elements (*i.e.*, $\mathcal{N} = 16$) that enforce the execution of handovers thanks to the high performance that can be reached. On the other side, in case of low values of ε, the associated handover probability will be lower as compared to the other trends (*e.g.*, see the black curves for $\varepsilon = 10^{-6}$). This means that there are small variations of BER of the serving link (*i.e.*, the direct ground-to-UE link), and then there will be no need to switch to a RIS-based ground-aerial-ground link. Finally, the trend variations noticeable from Fig. 12(*a*) to Fig. 12(*c*) are increasing for increasing RIS elements. Again, this is due since when $\mathcal{N}$ increases the link performance is better, and therefore a handover occurrence towards a no-direct RIS-based link is preferred. Finally, for comparison purpose in Fig. 13

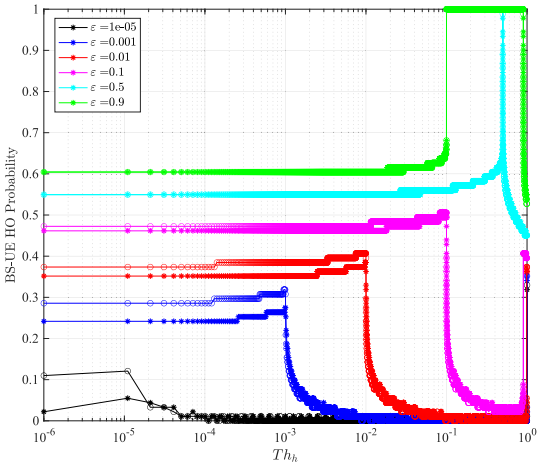

Fig. 13. Traditional (*i.e.*, no RIS-aided links) handover probability from BS1-to-UE (*asterisk markers*) to BS2-to-UE (*circle markers*) link in case of ping-pong effect, for different values of ε. Markers refer to MC simulations. Parameters are from CASE 1A.

we show the handover probability in case of direct ground links to prevent the ping-pong effect. The handover probability has a more dynamic behavior, with increasing trends for high ε values and smoother decreasing slopes, as well as lower handover probability values. This means that, in order to limit the ping-pong effect, the handover probability from a direct ground link to another ground link is lower than the handover toward a RIS-based BS-HAPS-UE link. For instance, for $\varepsilon = 10^{-4}$ (blue curve) the handover probability in case of no-direct ground-aerial-ground link in Fig. 12(*a*) is higher than that for direct ground-to-ground link shown in Fig. 13.

IX. Conclusion

This paper highlights how to benefit of using RISs for handover management in next generation wireless networks. The approach of traditional handover, which consists in switching from a serving AP to a candidate one, can be enhanced by redirecting the connectivity link from the serving AP to a RIS and then to the destination. We have defined specific scenarios where traditional handover is overcome by RIS-aided handover considering a variable number of RIS elements. By using

the error performance of various communication links, a new algorithm is developed for handover decision. It highlights when RIS-based handover is preferred to traditional handover.

The importance of RISs on the performance of RF link is presented depending on various link configurations and parameters. Results show that the handover probability through RIS is higher than that achieved with traditional handover, as well as relay-based link. RIS-assisted NLoS links can also be used for cell breathing to reduce the traffic load of cellular networks, as well as to avoid the ping-pong effect.

REFERENCES

[1] X. Yuan, Y.-J. A. Zhang, Y. Shi, W. Yan, and H. Liu, "Reconfigurable-intelligent-surface empowered wireless communications: Challenges and opportunities," *IEEE Wireless Commun.*, vol. 28, no. 2, pp. 136–143, Apr. 2021.

[2] S. Basharat, S. A. Hassan, H. Pervaiz, A. Mahmood, Z. Ding, and M. Gidlund, "Reconfigurable intelligent surfaces: Potentials, applications, and challenges for 6G wireless networks," *IEEE Wireless Commun.*, vol. 28, no. 6, pp. 184–191, Sep. 2021.

[3] K. Zhi, C. Pan, H. Ren, K. K. Chai, and M. Elkashlan, "Active RIS versus passive RIS: Which is superior with the same power budget?" *IEEE Commun. Lett.*, vol. 26, no. 5, pp. 1150–1154, May 2022.

[4] J. R. Kazim, J. Rains, M. A. Imran, and Q. H. Abbasi, *Application and Future Direction of RIS*. Hoboken, NJ, USA: Wiley, 2022, ch. 9, pp. 171–188.

[5] Y. Zhu, B. Mao, Y. Kawamoto, and N. Kato, "Intelligent reflecting surface-aided vehicular networks toward 6G: Vision, proposal, and future directions," *IEEE Veh. Technol. Mag.*, vol. 16, no. 4, pp. 48–56, Dec. 2021.

[6] V. Loscrí, C. Rizza, A. Benslimane, A. M. Vegni, E. Innocenti, and R. Giuliano, "BEST-RIM: A mmWave beam steering approach based on computer vision-enhanced reconfigurable intelligent metasurfaces," *IEEE Trans. Veh. Technol.*, vol. 72, no. 6, pp. 7613–7626, May 2023.

[7] S. R. Alkaabi, M. A. Gregory, and S. Li, "Multi-access edge computing handover strategies, management, and challenges: A review," *IEEE Access*, vol. 12, pp. 4660–4673, 2024.

[8] W. U. Khan, A. Mahmood, C. K. Sheemar, E. Lagunas, S. Chatzinotas, and B. Ottersten, "Reconfigurable intelligent surfaces for 6G non-terrestrial networks: Assisting connectivity from the sky," *IEEE Internet Things Mag.*, vol. 7, no. 1, pp. 34–39, Jan. 2024.

[9] S. Alraih, R. Nordin, A. Abu-Samah, I. Shayea, and N. F. Abdullah, "A survey on handover optimization in beyond 5G mobile networks: Challenges and solutions," *IEEE Access*, vol. 11, pp. 59317–59345, 2023.

[10] K. W. S. Palitharathna, A. M. Vegni, P. D. Diamantoulakis, H. A. Suraweera, and I. Krikidis, "Handover management through reconfigurable intelligent surfaces for VLC under blockage conditions," in *Proc. IEEE Int. Symp. Circuits Syst. (ISCAS)*, Singapore, May 2024, pp. 1–5.

[11] L. Jiao, P. Wang, A. Alipour-Fanid, H. Zeng, and K. Zeng, "Enabling efficient blockage-aware handover in RIS-assisted mmWave cellular networks," *IEEE Trans. Wireless Commun.*, vol. 21, no. 4, pp. 2243–2257, Apr. 2022.

[12] S. Deb, S. K. Ghosh, and S. C. Ghosh, "MAB based network selection mechanism for URLLC users in RIS assisted network," in *Proc. IEEE 21st Int. Symp. Netw. Comput. Appl. (NCA)*, vol. 21, Boston, MA, USA, Dec. 2022, pp. 173–179.

[13] H. Wei and H. Zhang, "An equivalent model for handover probability analysis of IRS-aided networks," *IEEE Trans. Veh. Technol.*, vol. 72, no. 10, pp. 13770–13774, Oct. 2023.

[14] W. Hedhly, O. Amin, M.-S. Alouini, and B. Shihada, "Intelligent reflecting surfaces assisted hyperloop wireless communication network," *IEEE Trans. Mobile Comput.*, vol. 23, no. 5, pp. 4943–4955, May 2024.

[15] J. C. S. S. Filho and M. D. Yacoub, "Nakagami-m approximation to the sum of m non-identical independent Nakagami-m variates," *Electron. Lett.*, vol. 40, no. 15, p. 951, 2004.

[16] N. D. Chatzidiamantis, G. K. Karagiannidis, E. E. Kriezis, and M. Matthaiou, "Diversity combining in hybrid RF/FSO systems with PSK modulation," in *Proc. IEEE Int. Conf. Commun. (ICC)*, Kyoto, Japan, Jun. 2011, pp. 1–6.

[17] H. Wang et al., "Performance of wireless optical communication with reconfigurable intelligent surfaces and random obstacles," 2020, *arXiv:2001.05715*.

[18] I. S. Gradshteyn and I. M. Ryzhik, *Table of Integrals, Series, and Products*. New York, NY, USA: Academic, 2014.

[19] M. H. Samuh, A. M. Salhab, and A. H. A. El-Malek, "Performance analysis and optimization of RIS-assisted networks in Nakagami-m environment," 2020, *arXiv:2010.07841*.

[20] V. Adamchik and O. Marichev, "The algorithm for calculating integrals of hypergeometric type functions and its realization in REDUCE system," in *Proc. Int. Symp. Symb. Algebr. Comput.*, New York, NY, USA, 1990, pp. 212–224, doi: 10.1145/96877.96930.

[21] Wolfram Inc. (2023). *The Wolfram Functions Site*. Accessed: Dec. 3, 2023. [Online]. Available: https://functions.wolfram.com

[22] H. Jiang et al., "Hybrid far- and near-field modeling for reconfigurable intelligent surface assisted V2V channels: A sub-array partition based approach," *IEEE Commun. Mag.*, vol. 22, no. 11, pp. 8290–8303, Nov. 2023.

[23] R. C. Ferreira, M. S. P. Facina, F. A. P. D. Figueiredo, G. Fraidenraich, and E. R. D. Lima, "Bit error probability for large intelligent surfaces under double-Nakagami fading channels," *IEEE Open J. Commun. Soc.*, vol. 1, pp. 750–759, 2020.

[24] S. A. Tegos, D. Tyrovolas, P. D. Diamantoulakis, C. K. Liaskos, and G. K. Karagiannidis, "On the distribution of the sum of double-Nakagami-m random vectors and application in randomly reconfigurable surfaces," *IEEE Trans. Veh. Technol.*, vol. 71, no. 7, pp. 7297–7307, Jul. 2022.

[25] S. Yadav, A. K. Yadav, R. Gour, G. C. Alexandropoulos, and D. S. Gurjar, "Two-way communications empowered by reconfigurable intelligent surfaces and direct link: Outage analysis under hardware impairments and Nakagami-m fading," *Phys. Commun.*, vol. 64, Jun. 2024, Art. no. 102352.

[26] A. P. Prudnikov, Y. A. Brychkov, and O. I. Marichev, *Integrals and Series: Special Functions*, vol. 2. Boca Raton, FL, USA: CRC Press, 1986.

[27] A. Prudnikov, Y. A. Brychkov, and O. I. Marichev, *Integrals and Series: Elementary Functions*, vol. 1. New York, NY, USA: Gordon&Breach Sci. Publ., 1986.

[28] A. A. Kilbas, *H-transforms: Theory and Applications*. Boca Raton, FL, USA: CRC Press, 2004.

[29] L. C. Andrews and R. L. Phillips, *Laser Beam Propagation Through Random Media*, 2nd ed. Bellingham, WA, USA: SPIE Press, 2005.

[30] A. I. Zreikat, "Load balancing call admission control algorithm (CACA) based on soft-handover in 5G networks," in *Proc. IEEE 12th Annu. Comput. Commun. Workshop Conf. (CCWC)*, Las Vegas, NV, USA, Jan. 2022, pp. 0863–0869.

[31] X. Zhao, W. Zhang, and C. Wang, "A load prediction based virtual cell breathing scheme for LTE—A system," in *Proc. IEEE Mil. Commun. Conf.*, San Diego, CA, USA, Nov. 2013, pp. 1296–1301.

[32] K. Ghanem, H. Alradwan, A. Motermawy, and A. Ahmad, "Reducing ping-pong handover effects in intra EUTRA networks," in *Proc. 8th Int. Symp. Commun. Syst., Netw. Digit. Signal Process. (CSNDSP)*, Poznan, Poland, Jul. 2012, pp. 1–5.

[33] T. Inzerilli, A. M. Vegni, A. Neri, and R. Cusani, "A location-based vertical handover algorithm for limitation of the ping-pong effect," in *Proc. IEEE Int. Conf. Wireless Mobile Comput., Netw. Commun.*, vol. 16, Avignon, France, Oct. 2008, pp. 385–389.

[34] M. Pan, J. Hu, J. Yuan, J. Liu, and Y. Su, "An efficient blind Doppler shift estimation and compensation method for LEO satellite communications," in *Proc. IEEE 20th Int. Conf. Commun. Technol. (ICCT)*, Nanning, China, Oct. 2020, pp. 643–648.

[35] E. Pajala, T. Isotalo, A. Lakhzouri, and E. S. Lohan. (2006). *An Improved Simulation Model for Nakagami-m Fading Channels for Satellite Positioning Applications*. [Online]. Available: https://api.semanticscholar.org/CorpusID:1801559

[36] G. Rafiq, B. O. Hogstad, and M. Pätzold, "Statistical properties of the capacity of double Nakagami-m channels," in *Proc. IEEE 5th Int. Symp. Wireless Pervasive Comput.*, Modena, Italy, May 2010, pp. 39–44.

Open Access funding provided by 'Università degli Studi Roma Tre' within the CRUI CARE Agreement